Dedicated to innovation in aerospace

OPZuid
Europees Innovatieprogramma Zuid-Nederland

Provincie Noord-Brabant

Europese Unie
Europees Fonds voor Regionale Ontwikkeling

PUBLIC

NLR-CR-2018-365-RevEd-1 | January 2022

Evaluation of in-service active thermography for composite structures

WP2 NDI (Non-destructive Inspection) in-service

CUSTOMER: OPZuid (Operationeel Programma Zuid-Nederland)

Royal NLR - Netherlands Aerospace Centre

Dedicated to innovation in aerospace

Evaluation of in-service active thermography for composite structures

WP2 NDI (Non-destructive Inspection) in-service

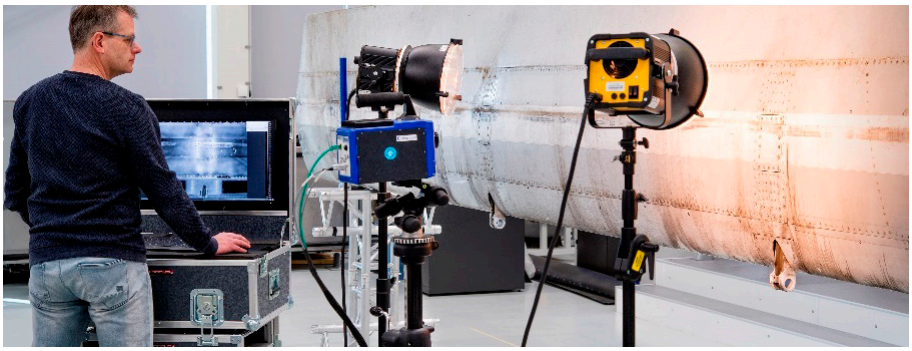

Thermography inspection on a B747 righthand inboard aft flap

REPORT NUMBER
NLR-CR-2018-365-RevEd-1

AUTHOR(S)
D.J. Platenkamp
H.P. Jansen

REPORT CLASSIFICATION
ONGERUBRICEERD

DATE
January 2022

KNOWLEDGE AREA(S)
Aerospace Structures
Testing

DESCRIPTOR(S)
Non-Destructive Inspection
Thermography
Composites
In-service
MRO

Problem area

The application of novel maintenance methods and availability of more accurate operational information is of key importance for the further reduction of aircraft down time, direct maintenance costs, predictability of aircraft availability and the everlasting need to improve price-performance ratio of aircraft operations and maintenance. Non-Destructive Inspection (NDI) is a vital link during Maintenance Repair and Overhaul (MRO) and further development of emerging inspection methods is crucial to keep maintenance efficient and cost effective. Within the framework of the Development Composite Maintenance Centre (DCMC), part of an OPZuid project, the novel NDI methods are further developed within Work Package 2 (WP2) to pursue this goal. Further, NLR knowledge, acquired within a broader multiannual framework, w.r.t. NDI is being used in WP2. The objective of WP2 is the development of reliable, fast and automated NDI method for large composite surface areas. Previous study, performed by the NLR, presented an overview of promising NDI methods which fulfils the objective of WP2. The down selection of NDI methods was based on technical characteristics and commercial aspects.

Description of work

Thermography was evaluated as a promising technique because of the non-contact nature, portability, fast operation, large Field Of View FOV (~1m^2), single sided access, all-in-all well suited for in-service inspections. The thermography method was evaluated on a thermoset material comprising a carbon composite solid and a sandwich laminate including the following damage types; impact damage, foil delaminations and skin-to-core disbonds. This report gives the results of an evaluation of Infrared Thermography Testing (IRT) method for in-service inspection of aircraft structures.

Results and conclusions

The assumptions of the research study are confirmed in this investigation. It is confirmed that the thermography inspection method is portable enough to operate under hangar conditions, operates fast, non-contact, has a large FOV (~1m^2), only needs a single sided access and is therefore well suited for in-service inspections. The method is only suitable for relative thin composite structures up to about 5-6 mm, depending on the acceptance criteria. The method is well capable of detecting impact damage, which is the most severe in-service damage that can occur to a composite structure. Inserted Teflon foils could be detected to a maximal depth of approximately 2mm. Possible reason that deeper positioned foils are not detected, is that the foils are adhered to the adjacent composite layers instead of a full separation of the individual laminate layers. This enables the transport of heat, leading to lower detectability. Larger skin-to-core disbonds (> 1inch) could be detected reliably. The detectable defect size decreases with increasing defect depth (defect diameter must exceed its depth). In general the lock-in thermography demonstrated a somewhat better performance compared to the pulse thermography method, the lock-in method also shows slightly better signal-to-noise ratio. Summarizing, the thermography is a cost effective inspection method for first screening of large composite areas for both solid and sandwich structures. When more detailed information is needed, the ultrasonic method can be used at anomalous areas appointed by the thermography inspection.

Applicability

This study has shown that the thermography method is a complementary NDI method and very well suitable to perform in-service inspections under hangar conditions. This result provides DCMC partners direction to further develop thermography inspection methods for composite in-service inspection.

Royal NLR
Anthony Fokkerweg 2
1059 CM Amsterdam, The Netherlands
p) +31 88 511 3113
e) info@nlr.nl i) www.nlr.nl

Dedicated to innovation in aerospace

OPZuid
Europees Innovatieprogramma Zuid-Nederland

Provincie Noord-Brabant

Europese Unie
Europees Fonds voor Regionale Ontwikkeling

PUBLIC

NLR-CR-2018-365-RevEd-1 | January 2022

Evaluation of in-service active thermography for composite structures

WP2 NDI (Non-destructive Inspection) in-service

CUSTOMER: OPZuid (Operationeel Programma Zuid-Nederland)

AUTHOR(S):

D.J. Platenkamp NLR
H.P. Jansen NLR

Royal NLR - Netherlands Aerospace Centre

CUSTOMER	**OPZuid (Operationeel Programma Zuid-Nederland)**
CONTRACT NUMBER	**31B1.0730 (PROJ-007230)**
OWNER	**NLR**
DIVISION NLR	**Aerospace Vehicles**
DISTRIBUTION	**Unlimited**
CLASSIFICATION OF TITLE	**UNCLASSIFIED**

APPROVED BY:		**Date**
AUTHOR	D.J. Platenkamp H.P. Jansen	28-01-2022 31-01-2022
REVIEWER	J.S. Hwang	31-01-2022
MANAGING DEPARTMENT	P. Arendsen	31-01-2022

Summary

The application of novel maintenance methods and availability of more accurate operational information is of key importance for the further reduction of aircraft down time, direct maintenance costs, predictability of aircraft availability and the everlasting need to improve price-performance ratio of aircraft operations and maintenance. Non-Destructive Inspection (NDI) is a vital link during Maintenance Repair and Overhaul (MRO) and further development of emerging inspection methods is crucial to keep maintenance efficient and cost effective. Within the framework of the Development Composite Maintenance Centre (DCMC), part of an OPZuid project, the novel NDI methods are further developed within Work Package 2 (WP2) to pursue this goal. Further, NLR knowledge, acquired within a broader multiannual framework, w.r.t. NDI is being used in WP2. The objective of WP2 is the development of reliable, fast and automated NDI method for large composite surface areas.

A research study was performed by the NLR [1] to get an overview of promising NDI methods which satisfy the requirements established in WP2. The down selection of NDI methods was based on the following inspection characteristics: the performance for defect detection, characterisation of the defects (size and depth), portability of the equipment, Field Of View (FOV), automatization/inspection speed, safety issues and costs of the equipment. The following NDI methods were selected for further evaluation: Laser Ultrasonic (LU), Infrared Thermography (IRT), laser shearography and X-ray backscatter technique. For LU testing, a round robin test will be performed within WP2 evaluating equipment's from different manufactures [2]. For laser shearography, an evaluation of the NDI methods will be performed by the NLR [3]. This report provides the results of an evaluation of IRT method for in-service inspection of aircraft structures. From a technical point of view the X-ray backscatter technique is an interesting technique. However, the current equipment costs (ROM > 500,- k€) are considered too high to fulfil the requirements of a cost effective inspection.

The evaluation of the IRT has been conducted on various composite reference panels (monolithic and sandwich), containing artificial defects (foils and disbonds), impact damages and water ingress. The evaluation of thermography showed, that the method is well capable of detecting impact-induced damage. Such damage can be a severe in-service damage mode that can occur to a composite structure. The method is in general suitable for relative thin composite structures up to about 5-6 mm. When thick-walled structures are inspected, the minimum detectable defect size will increase. Moreover, the study has shown that aforementioned defect types could only been found relatively close to the inspection surface (max. 2.0 mm depth). The larger skin-to-core disbonds (> 1 inch) at a depth of 3 mm could be detected reliably by the thermography method.

Thermography equipment is relatively portable and it operates contactless. Furthermore, it has a large FOV (~1 m^2) and it only requires a single sided access. Therefore, thermography is well suited for in-service inspections. By transforming the time-domain thermal data into frequency-domain data after a Fast Fourier Transformation (FFT) or a Discrete Fourier Transform (DFT), disturbances, such as reflections from the surface and thermal imbalance from the inspection room, can be attenuated for a great part. For these reasons, the thermography method is found to be well suited for inspections under hangar conditions.

Contents

Abbreviations

ACRONYM	DESCRIPTION
CFRP	Carbon Fiber Reinforced Polymers
DCMC	Development Centre for Maintenance of Composites
DFT	Discrete Fourier Transform
FFT	Fast Fourier Transform
FOD	Foreign Object Damage
FOV	Field Of View
IRT	Infrared Thermography
LPT	Long Pulse Thermography
LU	Laser Ultrasonic
LWIR	Long Wave Infrared
MRO	Maintenance, Repair and Overhaul
MWIR	Middle Wave Infrared
NDI/NDT[1)]	Non-Destructive Inspection / Non-Destructive Testing
NETD	Noise Equivalent Temperature Difference
NIR	Near Infrared
NLR	Royal NLR - Netherlands Aerospace Centre
OLT	Optical Lock-in Thermography
OPZuid	Operationeel Programma Zuid-Nederland
PT	Pulse Thermography
ROI	Region Of Interest
SNR	Signal to Noise ratio
SWIR	Short Wave Infrared

[1)] Non-Destructive Inspection (NDI) and Non-Destructive Testing (NDT) are often used by various publications. NDT and NDI refers to a testing and analysis technique to evaluate the properties of a material, component, structure or system for characteristic differences, defects and discontinuities without changing the property and integrity of the original part.

1 Introduction

The Development Centre for Maintenance of Composites (DCMC) has started in 2016 at industry park Aviolanda situated in Woensdrecht. The objective of DCMC is to cluster knowledge with respect to Maintenance Repair and Overhaul (MRO) of composite structures. The DCMC research program consists of seven Work Packages (WP), containing topics with respect to composite repair and inspection:

- WP1: Patchbond “development and certifying of composite bonded repair”
- WP2: Non-Destructive Inspection (NDI), in-service
- WP3: Improved rotor blade balancing
- WP4: Non-Destructive Inspection (NDI), thick composite structures
- WP5: Field & onsite repairs of composite structures
- WP6: Automated laser preparation for a composite bonded repair
- WP7: Fieldlab organisation and facilities

A research study was performed by the NLR [1] to get an overview of promising Non-Destructive Inspection (NDI) methods which satisfy the requirements stated in WP2. The down selection of NDI methods was based on the following inspection characteristics: the performance for defect detection, characterisation of the defects (size and depth), portability of the equipment, Field Of View (FOV), automatization/inspection speed, safety issues and costs of the equipment. The following NDI methods were selected for further evaluation: Laser Ultrasonic (LU), Infrared Thermography (IRT), laser shearography and X-ray backscatter technique. For LU testing, a round robin test will be performed within WP2 evaluating equipments from different manufactures [2]. For laser shearography, an evaluation of the NDI methods will be performed by the NLR [3]. This report provides the results of an evaluation of IRT method for in-service inspection of aircraft structures. Although from a technical point of view the X-ray backscatter technique is an interesting technique the current equipment costs are considered too high (ROM > 500,- k€) to fulfil the requirements of a cost effective inspection. Table 1-1 shows an overview of the performance of the selected NDI methods.

Table 1-1: Overview of the performance of the selected NDI methods [1]

Inspection Characteristic		**NDI methods**			
		Laser UT	**IR thermography**	**Laser shearography**	**X-Ray backscatter**
Defect detection	Impact	++	+	+	+
	Delamination / disbond	++	+[1]	0[1]	0[2]
	Kissing bond	0[3]	-	-	-
	Water ingress	0	+	-	+
Defect sizing		++	+	+	+
Depth estimation		++	0[4]	-	-
Portability equipment		-	0	0	-
Field Of View		+[5]	+	0	0
Inspection speed		+	++	+	+
Safety aspects		0	+	0	-
Investment costs		> 500 k€[6]	< 500 k€	< 500 k€	> 500 k€

The colours in the table give a rough qualification of the evaluation parameters for the different NDI methods (green – positive, yellow – with limitation, red – negative).
Note: 1 – for relative thin material (thickness < 5 mm), 2 – orientation depended w.r.t. the X-ray beam, 3 – non-linear UT or UT frequency analyses, 4 – TSR or PPT technology, 5 – using scan system, 6 – trending less expensive equipment in development

This report gives the results of an evaluation of two Infrared Thermography methods namely; the Optical Lock-in Thermography (OLT) and Pulse Thermography (PT), both suited for in-service inspection of composite structures. Its damage detection and quantification characteristics will be evaluated by means of two reference panels. Chapter 2 starts by first defining the relevant in-service defects that can be found in a composite structures. Chapter 3 presents the two reference specimens with relevant information on defects. Chapter 4 explains theories behind the thermography inspection. The test results will be presented in Chapter 5. Thereafter, the results will be discussed and conclusions will be drawn in Chapter 6 and 7 respectively.

2 Definition of in-service damage

In general it can be observed that Carbon Fiber Reinforced Polymers (CFRP) are widely used in light-weight structures. From the aerospace point of view, the new aircraft types, such as F-35, NH-90, B787 and A350, are examples of large-scale application of CFRP. Moreover, other non-aerospace sectors, e.g. the automotive, maritime, civil engineering, energy (wind turbines) and infrastructure, show trending of increased CFRP applications for its light weight structures. Due to this increase of need for CFRP materials, demand for fast and cost-effective NDI techniques during in-service of the component also increases. To select the appropriate NDI technique, it is important to know what kind of damage types can occur during the service life of a component. Table 2-1 gives an overview of typical defect types which can occur in composite material during the different stages of the manufacturing process and in-service life. For the in-service inspection of a composite structure, knowledge of the production process and the end product is essential, especially the defect types, which can be present in an accepted composite structure. The last column gives the overview of the defect types which can occur during service life of a composite structure. Especially delamination (e.g. caused by Foreign Object Damage (FOD)) is a relevant defect type because impact damage is generally considered as the type of in-service damage most significantly affecting the structural strength.

Table 2-1: Typical defect types composite material

Typical defect types composite material			
Incoming material:	During manufacturing	Final composite structure	In-service defects
Contaminations	Contaminations	Delamination	Delamination
Damaged filaments	Damaged filaments	Edge defects	Edge defects
Fiber misalignment	Edge fraying	Foreign object	Disbond
Fuzz balls	Fiber misalignment	In-plane fibre waviness	Kissing bond
Gaps	Fuzz balls	Micro cracks	Surface defects
Missing roving	Gaps	Out-of-plane fibre waviness	Water ingress
Warp deviation	Missing roving	Porosity	
Weft deviation		Resin rich areas	
Skewing		Surface defects	
Crease, wrinkle, wavy cloth		Void	
Broken filaments Local fiber or weave distortions, Fuzz balls, broken selvedge			
Yarn splices (Warp/Weft)			
Excess binder, binder gaps			

3 Composite specimen configurations

For the purpose of the IRT evaluation study, two specimens were selected which represents composite structures related to the aerospace sector. The test specimens comprise of a solid laminate (called specimen A2) and a sandwich structures (called specimen C). Both specimens have no stiffeners. The damage types in the test components are impact induced delaminations, foils, disbonds and water ingress. The two specimens are both thermoset material, the sandwich specimen contains a Nomex honeycomb core with thickness of 19 mm and cell size of 0.25 inch. Table 3-1 shows the "general" thermal material properties of the selected specimens, a brief definition of these thermal material properties is given in Chapter 4.

Table 3-1: General thermal material properties of the specimens, values are taken from literature

Material	Specific heat (kJ/KgK)	Thermal conductivity (W/mK)	Density (kg/m^3)	Thermal diffusivity (mm^2/s)	Thermal effusivity (W sqrt(s) / m^2 K)
Carbon fabric	1100	0.7	1528	0.42	1084
Nomex core	1200	0.13	24	4.51	62
Teflon foils	1000	0.24	2200	0.11	726.64
Copper	390	401	8960	115	37433
Air (thin gaps)	1005	0.07	1.2	58.04	9
Water	4193	0.586	1000	0.14	1567.51

The specimens were provided with artificial delaminations and/or disbonds by inserting Tygavac TFG 075/1 foils (Fothergill Tygaflor Ltd., Littleborough, England) in the laminates during the manufacturing stage. Tygavac TFG 075/1 is a non-porous PTFE (Teflon) coated glass fabric with a nominal thickness of 0.075 mm.

The two specimens are partly covered by a copper wire mesh (embedded in the resin of the surface layer).
This material is a surface protection system and is often used in composite structures for lightning strike protection.
The copper wire mesh is a plain weave fabric with a wire distance w of 0.458 mm and a wire diameter d of 0.053 mm, see Figure 3.1.

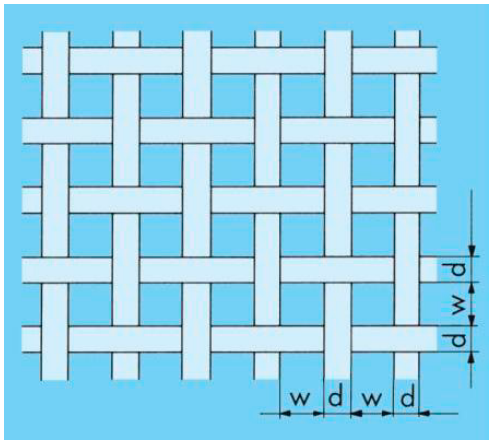

Figure 3.1: Schematic of the copper wire mesh used for the reference specimens

3.1 Specimen A2

Specimen A2 is a solid laminate with dimensions of 900 x 600 mm. The thickness of specimen A2 is overall 5.4 mm. The laminate consists of 24 layers with quasi-isotropic lay-up. Half of the specimen is covered with a copper wire mesh, simulating the lightning protection. For an overview of the specimen, see Figure 3.2. Both parts of the specimen (with/without cupper mesh) contain the following internal defects:

- Interply delaminations, simulated by Teflon foils of diameter 0.25, 0.5 and 1 inch, and placed at three different depths (0.7, 3.4 and 4.7 mm).
- Natural delaminations, caused by impacts with different energy levels and tub diameters. Ultrasonic data gives information about the appearance and size of the delaminated areas, see Figure 3.3.

For orientation purposes, adhesive stickers are applied with a diameter of 8 mm both on the top and bottom side and hole D with a diameter of 8 mm.

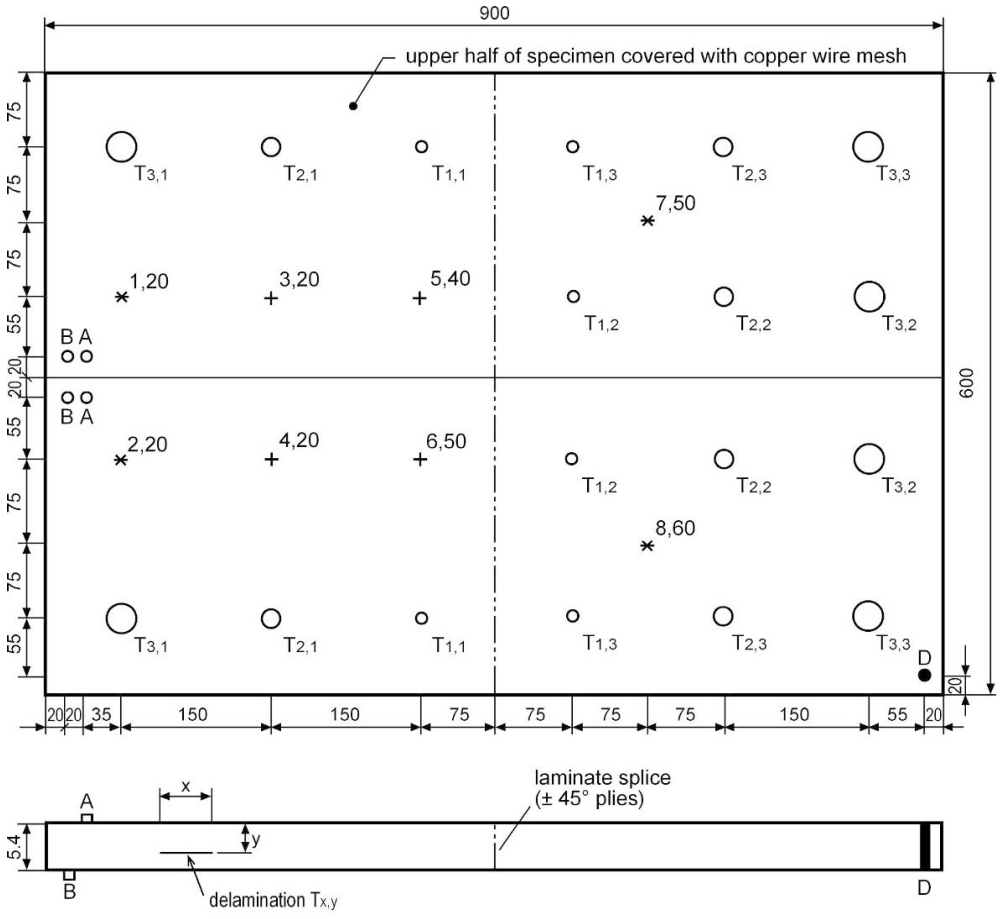

Defect type	
Delamination $T_{x,y}$	x = 1, 2 or 3 Diameter 0.25; 0.5 or 1.0 inch y = 1, 2 or 3 Depth 0.7; 3.4 or 4.7 mm
Impact $+^{x,y}$ $*^{x,y}$	+ / * Impactor tup diameter 0.5/1.0 inch x = Impact number; y = Impact energy [J]
Adhesive sticker	A ∅ 8 mm on top side of laminate B ∅ 8 mm on bottom side of laminate
Hole D	∅ 8 mm

Figure 3.2: Specimen A2, structural details solid laminate thickness 5.4 mm

To determine the size of the impact damage an ultrasonic pulse-echo measurement is made, the C-scan test results can be seen in Figure 3.3 including the width and height dimensions.

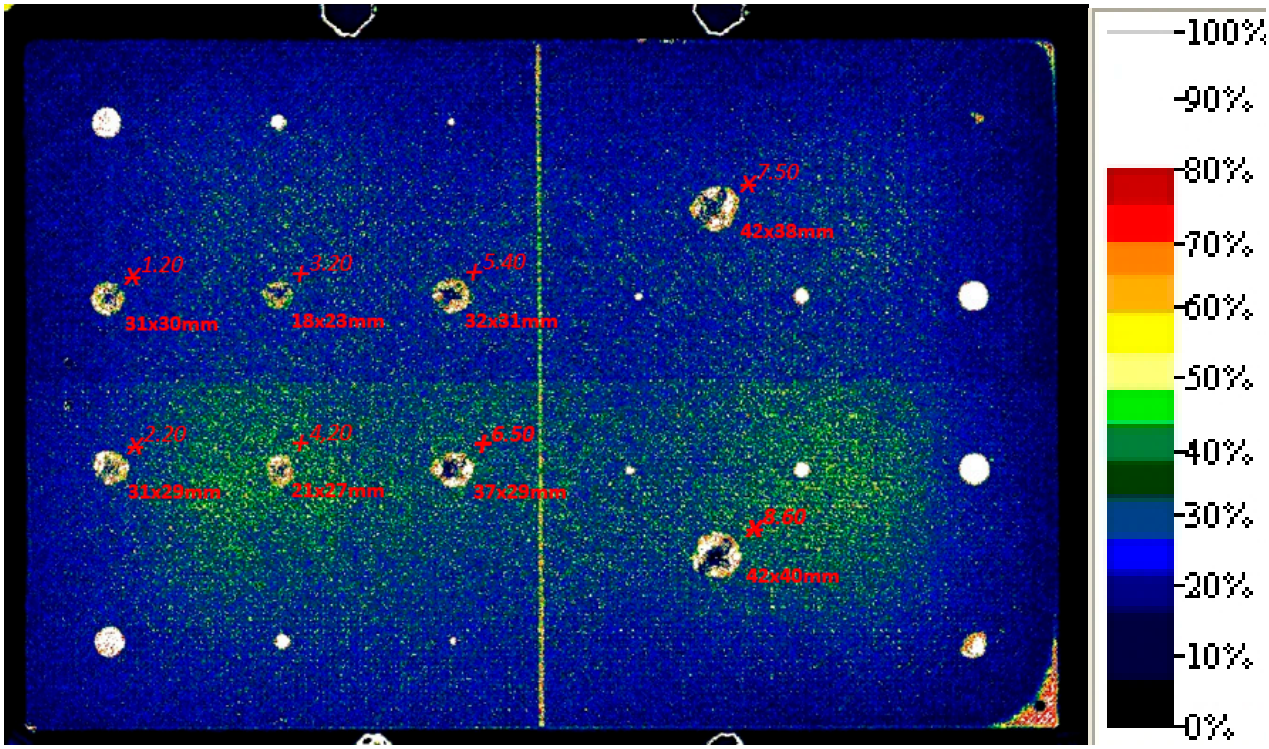

Figure 3.3: Specimen A2, ultrasonic pulse-echo reflection data (gate between front and backwall reflection) of the impact damage locations

3.2 Specimen C

Specimen C is a sandwich structure with dimensions of 900 x 600 mm. The core consists of a Nomex honeycomb with thickness of 19 mm and cell size of 0.25 inch (6.4 mm). The outer and inner skins thickness are 3.0 and 1.5 mm respectively. The outer skin laminate is 12 layers with quasi-isotropic lay-up. The inner skin laminate is 6 layers with quasi-isotropic lay-up. Half of the outer skin laminate is covered with a copper wire mesh. For an overview of the specimen see Figure 3.4. Both parts of the specimen (with/without copper mesh) contain the following internal defects:

- Interply delaminations in the outer skin simulated by Teflon foils of diameter 0.25, 0.5 and 1 inch, and placed at two different through-the-thickness positions (depths of 1.5 and 2.25 mm);
- Outer skin-to-honeycomb core disbonds simulated by flat-bottomed holes in the Nomex core of diameter: 0.25, 0.5, 1 and 2 inch;
- Natural delaminations caused by impacts with different energy levels and tub diameters. Ultrasonic data gives information about the appearance and size of the delaminated areas;
- Water ingress in the Nomex honeycomb cells.

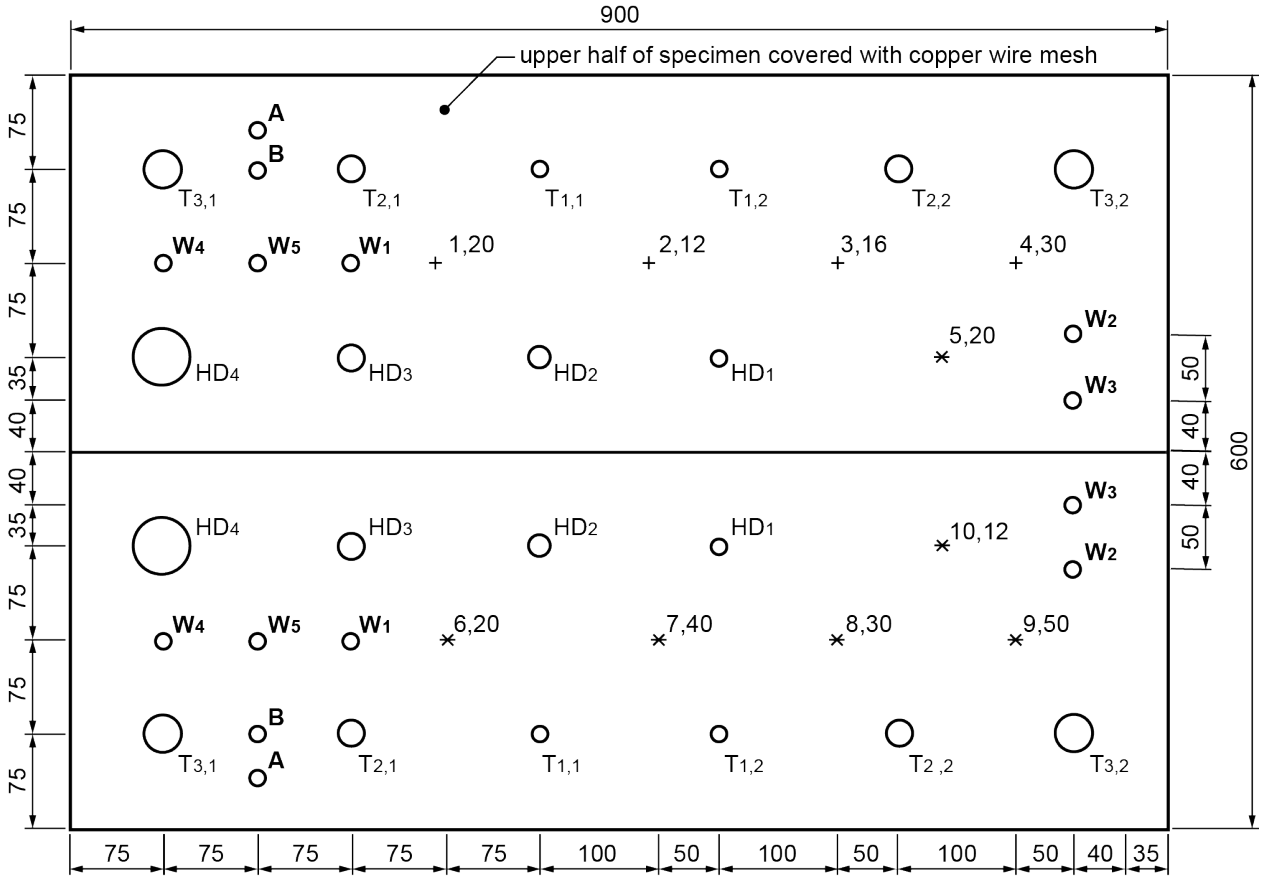

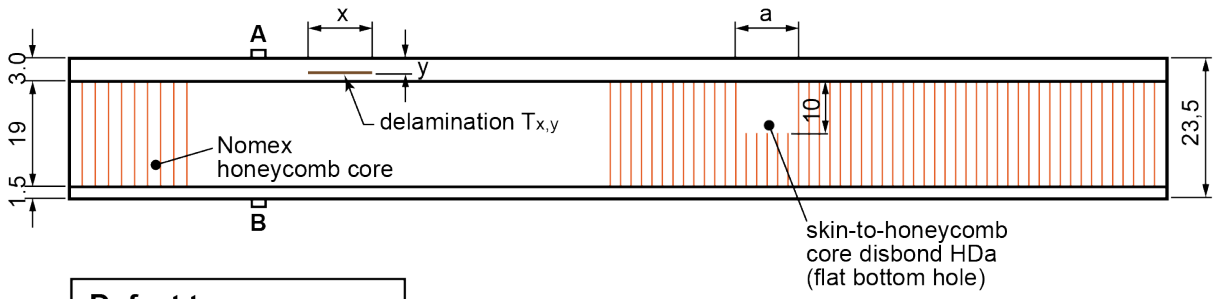

Defect type		
Delamination $T_{x,y}$	x = 1, 2 or 3 y = 1 or 2	Diameter 0.25; 0.5 or 1.0 inch Depth 1.5 or 2.25 mm
Skin-to-honeycomb core disbond HDa	a = 1, 2, 3 or 4	Diameter 0.25; 0.5; 1.0 or 2.0 inch
Impact $+^{x,y}$ $*^{x,y}$	+/* Impactor tup diameter 0.5/1.0 inch x = Impact number; y = Impact energy [J]	
Adhesive sticker	A ∅12 mm on outer skin B ∅12 mm on inner skin	
Water ingress Wx in honeycomb cells (HC)	x = 1 1 HC full x = 2 3 HC full x = 3 3 HC half-full x = 4 7 HC full x = 5 7 HC half-full	

Figure 3.4: Specimen C, structural details sandwich structure

To determine the size of the impact damage in the skin, an ultrasonic pulse-echo measurement is performed. The C-scan test results can be seen in Figure 3.5, including the width and height dimensions of the damages.

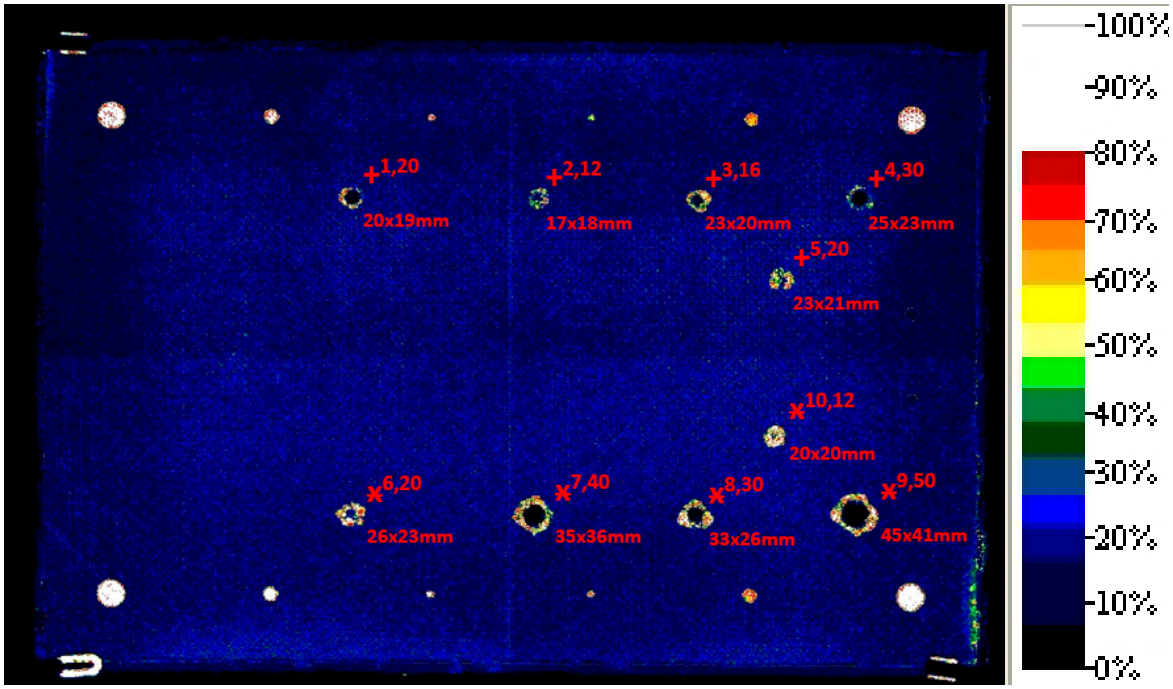

Figure 3.5: Specimen C, ultrasonic pulse-echo data reflection of the impact damage locations

Next to the delamination damage in the skin, also a skin-to-core disbond can occur. This type of damage can only be detected with the ultrasonic through-transmission technique, for which two sided access is needed. The size of the skin-to-core disbond can be seen in Figure 3.6. On the other hand, the through-transmission C-scan data does not shows a complete attenuation of the sound beam at the impact location. This is an indication that the core is not completely separated from the skin.

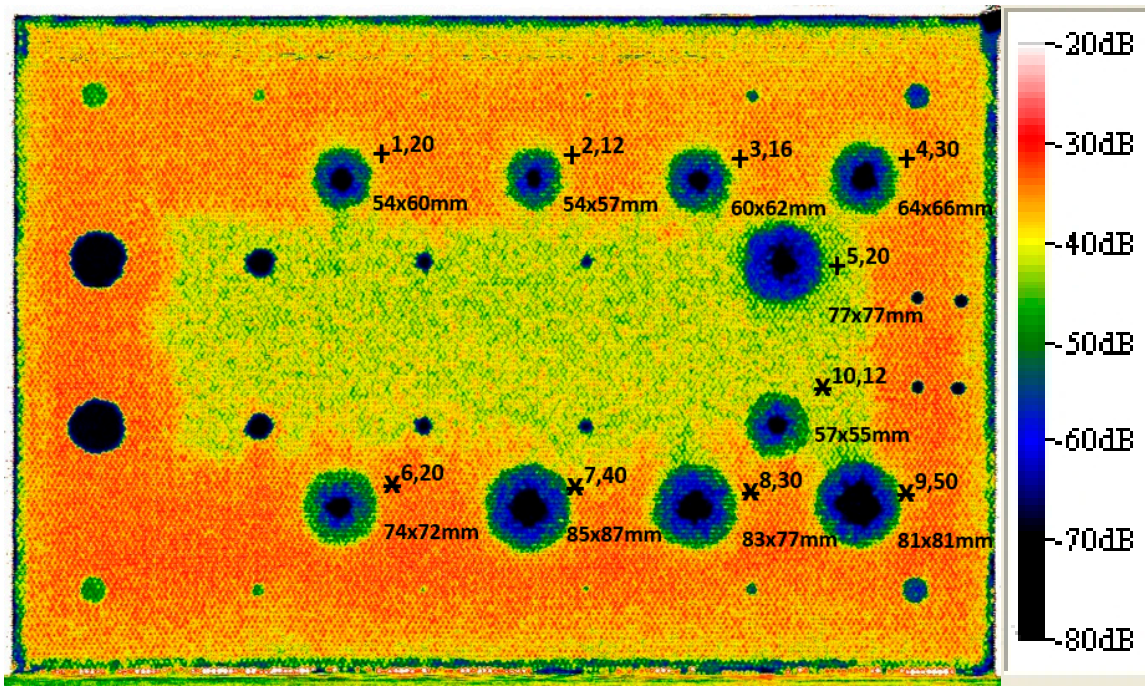

Figure 3.6: Specimen C, ultrasonic through-transmission data of the impact damage locations

4 InfraRed Thermography (IRT)

InfraRed Thermography (IRT) is a non-contact NDI method that measures the heat radiation pattern on the surface of a test part. The method employs light with wavelengths just above the visible part of the electromagnetic spectrum, in the range of about 0.9 – 14 µm, see Figure 4.1. There is no consensus on the division of the bands, but for this report we will use the band typically used by camera manufactures.

- Near Infrared (NIR) from 0.7 to 1 µm.
- Short Wave infrared (SWIR) from 0.9 – 1.7 µm.
- Middle Wave infrared (MWIR) from 3-5 µm.
- Long Wave infrared (LWIR) from 8-15 µm.

IRT can be divided into passive and active techniques. Passive IRT uses heat generated by natural (e.g. sun) or its internal heat source. Active IRT uses external stimulus source to impose heat on the surface of the object. In general, the active technique is used for NDI purposes.
Active IRT involves temperature measurement of object surfaces that are subjected to a thermal excitation. This thermal excitation can for example be applied by halogen lamps, piezo elements or laser excitation. When an object has a constant surface temperature (thermal equilibrium), it is not possible to detect possible deviations. When an object is excited, either by an external heat source or by mechanical vibrations, the differences in surface temperature are caused by internal features (discontinuities/geometry). For the NDI application, it is not necessary to measure absolute surface temperatures but only temperature differences. Knowledge of the internal geometry of the object inspected is mandatory to differentiate between the temperature contrast caused by defects and geometrical features.
Thermographic techniques are well applicable in composite materials because of their relatively low thermal conductivity (< 1 W/m·K). This implies a slow lateral heat flow with closely spaced isotherms, resulting in a good defect resolution. In general, the flaw size must be larger than the depth of the flaw in order to be detected by IRT. IRT is capable of inspecting surface areas up to 1 m^2 in a single inspection.

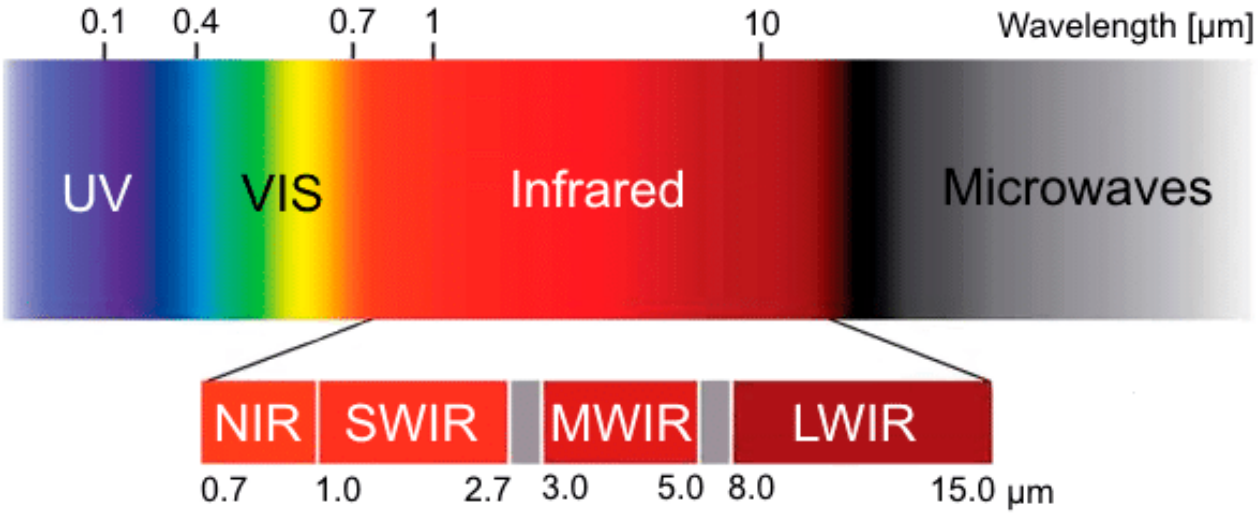

Figure 4.1: Electromagnetic spectrum with the infrared region highlighted showing the NIR, SWIR, MWIR and LWIR regions [4]

Besides the different types of thermography, also a different excitation sources can be used: optical light sources (halogen/flash lamps), laser, induction and ultrasound. For this study, only excitation by optical means (lamps) are discussed. This chapter explains the theory of heat, radiation and how these phenomena are used for IRT. Thereafter, two active IRT methods, namely OLT and PT, will be explained. Section 4.1 summarizes heat transfer theorem to provide the reader with better understanding about thermal behaviour in a material. Section 4.2 presents more information on one of three heat transfer mechanism, which is used in IRT. In this study, Optical Lock-in Thermography (OLT) and the Pulse thermography (PT) are used to inspect the two composite reference specimens. The techniques are described in Section 4.3 and 4.4, respectively. Section 4.5 presents data analysis algorithms for IRT inspection data.

4.1 Heat Transfer Theory

To have a better understanding about thermal behaviour in a material, it is important to know the differences between temperature and heat. A material contains molecules which are the basic building blocks; hotter molecules will move faster than cooler molecules. The speed of the molecules will correspond to a certain temperature level. With materials above absolute temperature (-273°C), the molecules will move resulting that the object will emit some form of energy, this is called heat.
For both thermal material properties a short definition:

Heat: The amount of heat in an object is the total kinetic energy of the molecules. Specific heat [c_p] is that amount of thermal energy that is needed to increase 1 kg of material with one Kelvin, in J/(kg K).

Temperature: Is a measure of the average speed of the molecules and the atoms, in K.

When two materials at different temperatures are in contact with each other or they are close to each other, the warmer object will transfer energy to the colder object until equilibrium is established. Heat can be transferred by three different mechanisms:

- Conduction, materials are in mechanical contact with each other;
- Convection, a fluid transfers heat due to convection;
- Radiation, materials receive and emit thermal radiation.

Conduction is a heat transfer mechanism occurring between two bodies standing in physical contact with different temperatures. Due to the dynamics of molecules, the kinetic energy of molecules is transferred from a body with high temperature to other body with lower kinetic energy (low temperature). When a hot object is surrounded by a fluid that is colder, the fluid will heat up in proximity of the object. A fluid with a higher temperature will have a lower density causing it to rise, due to gravity. This will result in convection currents cooling down the surface. The third method is heat transfer by radiation and this will be discussed in more detail in Section 4.2.

The rate of transfer of heat of a material from the hot end to the cold end is called the thermal diffusivity α, expressed in [m^2/s]. Thermal diffusivity of a material can be calculated as:

$$\alpha = \sqrt{\frac{\lambda}{\rho c_p}} \tag{4.1}$$

The following material properties are of importance:

- Heat conductivity λ, the ease at which heat is conducted inside of the material, expressed in [W/(m·K)];
- Density ρ of the material, expressed in [kg/m^3];

- Specific heat capacity c_p, the amount of energy needed to heat up 1 kg of the material by 1 degree , expressed in [J/(kg·K)].

The materials ability to exchange thermal energy with its surroundings is represented as thermal effusivity e, expressed in [W$\sqrt{s}$/(m^{2}K)]. Thermal effusivity is also called thermal inertia or thermal responsivity of the material. The thermal effusivity of a material can be calculated as:

$$e = \sqrt{\lambda \rho c_p} \tag{4.2}$$

In order to better explain these properties, two common materials, wood and steel, will be used as an example in the following discussion. The properties of these materials are given in Table 4-1.

Table 4-1: Thermal properties of wood and steel

Material	Heat conductivity λ (W / m K)	Density ρ (kg / m^3)	Specific heat capacity c_p (J / kg K)	Thermal diffusivity α (mm^2 /s)	Thermal effusivity e (W$\sqrt{s}$/m^2 K)
Wood (Pine)	0.13	420	1500	0.21	286
Steel (ST52-3)	40	7850	420	12.13	11483

Wood has a lower conductivity than steel, is less dense and has a higher specific heat capacity, resulting in a lower thermal diffusivity as compared to steel. When a wooden and a metal spoon are put in a pan of boiling hot water the metal spoon will warm up much faster than the wooden spoon, due to the higher thermal diffusivity. Eventually, over time, and neglecting convective and radiation cooling effects, both spoons will have the same temperature as the boiling water. When a person touches the spoons, which are at the same temperature, the wooden spoon will feel much colder than the metal spoon. The action of touching a spoon will cause the temperature of your skin to increase while the temperature of the spoon decreases. The temperature at the contact point can be calculated with the following formula:

$$T_m = T_1 + (T_2 - T_1)\frac{e_2}{e_2 + e_1} \tag{4.3}$$

where T_m is the temperature in the middle, at the contact point. T_1 and T_2 are the temperature of material 1 and 2, respectively. Further, e_1 and e_2 are the effusivity of material 1 and 2. The temperature at the contact point depends on the temperature of the material and the thermal effusivity of the material. If we take human skin (T_1 = 25°C e_1 =890 (W$\sqrt{s}$/m^2 K)) we can calculate the temperature at the contact point for both the spoons, resulting in 43°C for the wooden spoon and 94°C for the metal spoon. Due to the large thermal inertia (large e) of the metal spoon, the contact point remains much hotter as compared to the wooden spoon.

There are few remarks related to the thermal properties and the NDI with IRT.

- To be able to find defect with IRT on a composite structure, an important condition has to be satisfied. The thermal properties of the defect area should deviate significantly (thermal contrast, large effusivity difference) compared to the relative uniform thermal material properties of “sound base material”.
- The thermal properties values of most metals are well defined and reproducible. On the other hand, the thermal properties of the CFRP materials, which contain non-isotropic material properties, are directionally dependant. which makes it rather difficult to apply thermal material property values found in literature.
- It is well known that the reproducibility of the thermal properties of the same CFRP material is lower than, for example, metals. This is caused due to the manufacturing tolerance on fibre volume fraction, undulations,

variation in voids, etc. Even though the mechanical property may fulfill the product specification, thermal property may vary due to these number of variables.

- Considering these remarks, the ability of the IRT technique to reliably detect the defects should be demonstrated experimentally for each composite material/product configurations.

4.2 Thermal Radiation

All objects with temperature above absolute zero (0 K) will emit thermal radiation, which is described by the Planck's law. When only looking at temperature influences (no material and environmental influences) in relation to the emitted energy of a blackbody, the following so-called Planck curves can be plotted which also shows the wavelength distribution, see Figure 4.2. The following can be observed:

- The curves have a similar shape and do not cross each other;
- At higher temperatures more radiation energy is emitted;
- The peak wavelength becomes smaller at higher temperatures;
- The peak wavelength becomes smaller at higher temperatures;
- As the wavelength shortens, it becomes in the visible range, so-called incandescence.

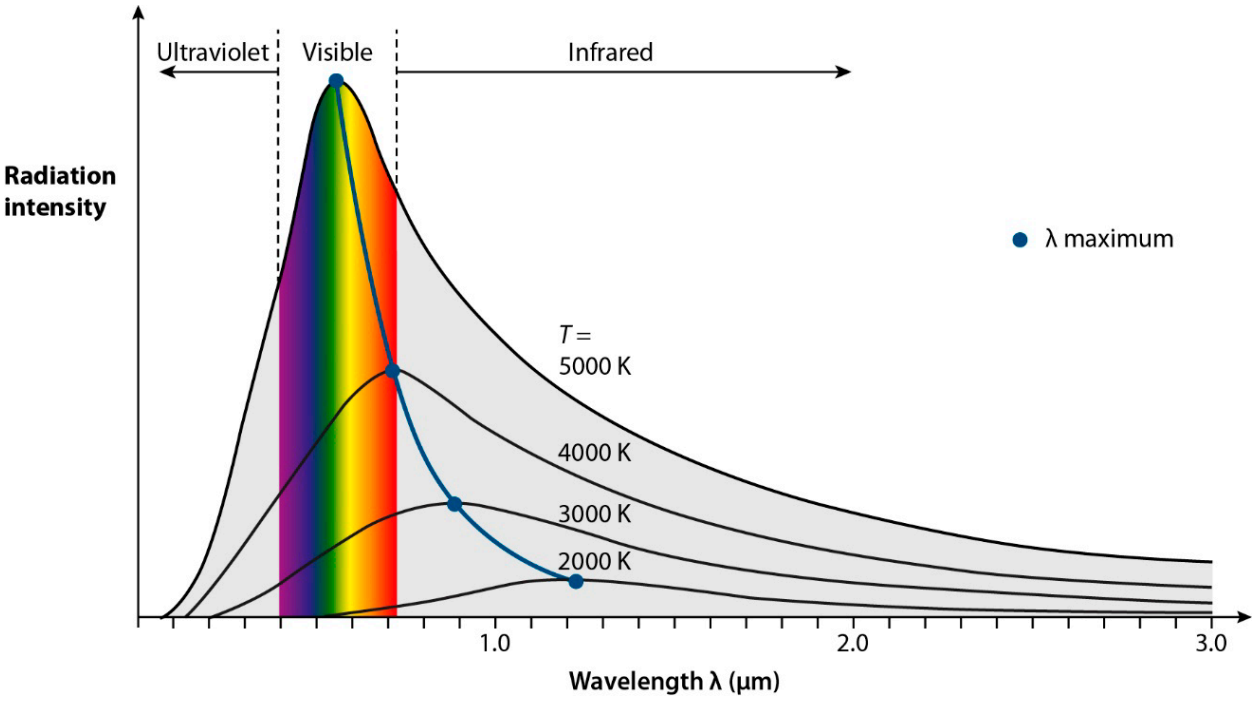

Figure 4.2: Blackbody emissive radiation power against the wavelength (Planck's law) (ref.web)

There are two formulas derived from the Planck's law which are useful for IRT inspection. The Stefan-Boltzmann formula calculates the total radiated power P [W/m^2] for a given temperature (area beneath the curve) expressed as

$$P = \sigma A \varepsilon T^4 \tag{4.4}$$

where σ is the Stefan-Boltzmann constant [W/m^2], A is the surface of the body [m^2], ε is emissivity (dimensionless between 0 and 1) and T is the temperature [K]. The wavelength associated with the maximum intensity (peak of the curve) λ_{max} [μm]can be calculated with the Wien's displacement law at a given temperature, the blue line in Figure 4.2.

$$\lambda_{max} = \frac{2898}{T} \tag{4.5}$$

To get a feeling about the Planck curves some examples of λ_{max}, the peak of the intensity:

Human: T=310K	λ_{max} = 9.35 (µm)	Not visible (in the far infrared)
Melted Iron T=1810K	λ_{max} = 1600 (µm)	Not visible (still the far infrared)
Incandescent light bulb T = 2800K	λ_{max} = 1035 (µm)	Not visible (still the far infrared)

The maximum radiation intensity of melted iron is in the infrared region and the human eye cannot see this radiation. This is also the case for an incandescent light bulb which we use for lightning. For both these situation, the maximum intensity are at wavelengths beyond the visible region. However, the objects still emit light in the visible part of the spectrum only with lower intensities, due to the broad peak. For the incandescent light bulb, most of the energy is emitted in the infrared region, which is why there are being replaced by more efficient LED lightning.

The emissivity is also used in the calculation of total power with the Stefan-Boltzmann formula, equation (4.4). Emissivity is defined as the ratio of the energy radiated from a material's surface to that radiated from a perfect emitter, known as a blackbody (ε = 1). Blackbodies are an idealized physical body that absorbs all incident electromagnetic radiation, regardless of frequency or angle of incidence. The name black body is given because it absorbs all colours of lights. A black body with an temperature above absolute zero will emit black-body radiation, as an ideal emitter at every frequency. Additionally, it is also a diffuse emitter, meaning that the energy is radiated isotopically. A figure of a blackbody emitter can be seen in Figure 4.3

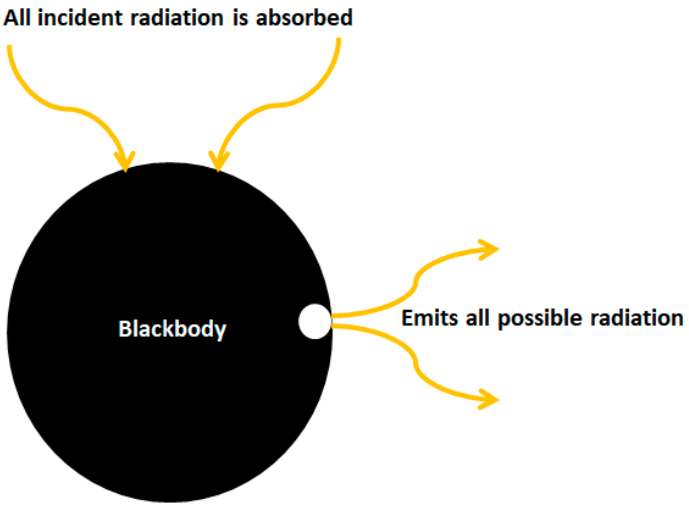

Figure 4.3: Principle of blackbody, emitted radiation is only a function of the blackbody temperature

Normal object are not ideal blackbodies (ε < 1), meaning that the amount of energy they emit will be lower as compared to an ideal blackbody. Additionally, the emissivity value will change depending on the frequency (wavelength) of the emitted radiation, therefore, $\varepsilon = \varepsilon(\lambda)$. A body that has an emissivity lower than one, but that is constant over the entire frequency spectrum is called a grey body. The emissivity value of an object is highly depend on the surface properties of that object. To give an example, Table 4-2 gives the emissivity values for aluminium with different surface properties.

Table 4-2: Emissivity values of aluminium

Material	Emissivity ε
Aluminium highly polished	0.04
Aluminium rough	0.07
Aluminium heavily oxidized	0.25
Aluminium anodized	0.77

Aluminium that is highly polished has a very flat surface and a low emissivity value of 0.04. If the surface becomes rougher, the emissivity value increases. For an oxidized surface, the emissivity value is about 6 times as high as compared to a polished surface, meaning that six times more energy will be emitted from that surface even when it has the same temperature as the polished surface. An anodized surface has an even higher emissivity.

All objects transmit, absorb, emit and reflect radiation. Glass is a material that transmits visible light, allowing you to see through windows. However, the window does not transmit in the infrared spectrum becoming opaque and impossible to see through. Transmission of IR radiation for most common objects does not happen at the infrared wavelengths used during an inspection, so it can be neglected .This leaves absorption, emission and reflection, which are all dependent on the emissivity of an object. In general, materials that have a low emissivity are bad absorbers, bad emitters and good reflectors. Other way around, materials with a high emissivity are good absorbers.

An infrared camera detects thermal radiation coming from an object. The total amount of radiation depends on the amount of reflected and emitted light, which both depend on emissivity. The total amount of emitted radiation depends not only on the emissivity of the object but also on its temperature. When electromagnetic radiation strikes an object surface (e.g. by halogen lamps in the case of IRT), absorption and reflection occurs. The energy that is absorbed is transferred to heat, thereby increasing the temperature of the part. The energy that is reflected does not heat up the part. Objects with low emissivity are difficult to heat up with halogen lamps, since a low amount of energy will be absorbed. A large part of the energy will be reflected. Therefore, care should be taken that the reflection of the halogen lamps do not enter the camera directly. The infrared camera will detect reflected radiation rather than emissive radiation from the object, leading to improper temperature readings. Additionally, other source of thermal radiation should not be present in the scene since the camera will detect the reflection of these sources from the object under investigation.

To measure absolute temperatures with an IR-camera, compensation for different emissivity values must be performed for correct absolute temperature readings. With the NLR thermography system, no absolute temperatures are measured, only differences in object radiation and the calibration is therefore not performed.

4.3 Optical Lock-in Thermography

Optical Lock-in thermography (OLT) uses a (low-frequency) sinusoidal modulated heating (Amplitude modulation (AM)) which is imposed on the test part using one or multiple sets of halogen lamps, see Figure 4.4 The test part is monitored with an infrared camera during the modulation cycle in order to obtain an image of amplitude and phase of the temperature response of the surface. When the modulated radiation hits the surface of the test part, a thermal wave is generated. This wave propagates into the interior where it is reflected at boundaries and defects (which exhibit other thermal properties), and finally returns back to the surface where it is superposed with the initial wave [5]. In general, the frequencies of the sinusoidal wave are in the range of approximately 0.5 – 0.005 Hz for composite material application.

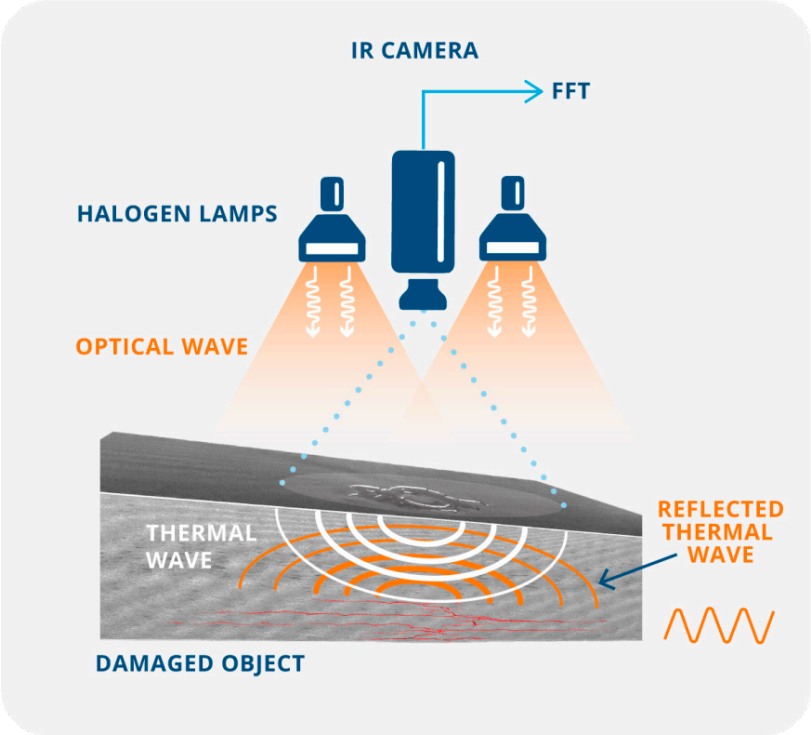

Figure 4.4: Principle of Optically excited Lock-in Thermography (OLT)

When the sinusoidal heating is imposed on the test part, there will be a temperature change. This change consist of a constant temperature increase (Direct Component - DC) and a periodic change in temperature (Alternate Component - AC), see Figure 4.5. After a certain time (number of cycles), the surface temperature will reach equilibrium state for the DC component, leaving only the AC component. At this equilibrium state, the most accurate IRT measurements can be performed. In practice, it is very hard to achieve this surface temperature equilibrium requiring long inspection times. Therefore, most OLT systems are measuring the temperature trend of the AC component.

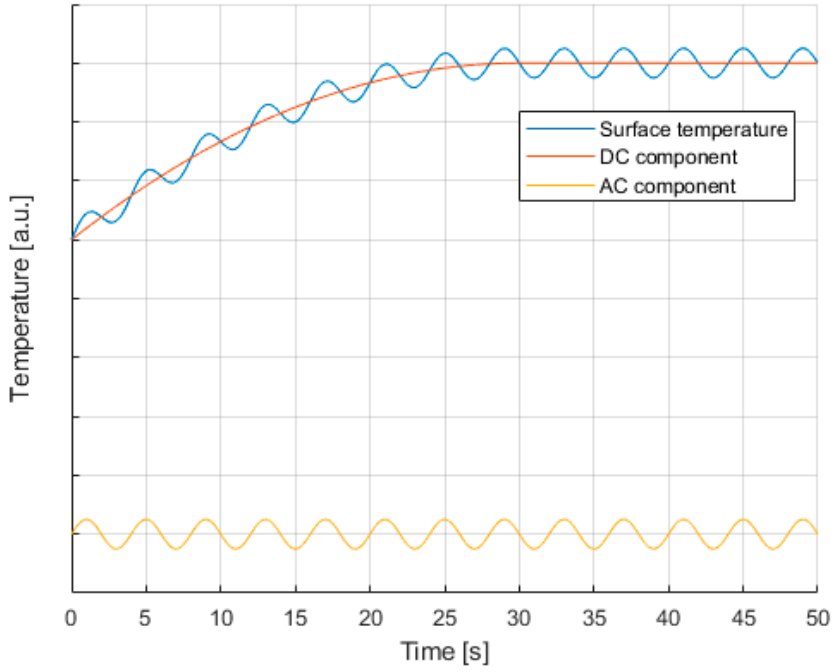

Figure 4.5: Example of a surface temperature profile with a constant temperature rise (DC) and the periodic deviation (AC)

In case of experimental trials, where repetitive measurements are performed on one specimen, the surface temperature can be constantly increased. This can lead to a saturated signal of the IR camera, due to the high temperature of the specimen. The AC component due to excitation will cause a variation in temperature, but this variation cannot be detected anymore by the camera. Cooling down of the specimen, changing shutter settings of the IR camera, or modifying the amplitude of the halogen lights can be used to overcome this problem.

With OLT, the periodic response is isolated and analysed in the frequency domain by performing a Fast Fourier Transform (FFT) on the captured signal. The frequency of the modulation determines the thermal penetration depth μ of the thermal waves into the material. The thermal penetration depth can be calculated using the following formula:

$$\mu = \sqrt{\frac{\alpha}{\pi f}} \tag{4.6}$$

where α is the thermal diffusivity of the material in [m^2/s] and f the modulation frequency in [Hz].
Figure 4.6 shows three different situation regarding penetration depth. Situation 1 is the case where the test consists of relatively thick composite material and the modulation frequency f_1 is relatively high. For situation 1, where the thickness of the part is larger than the penetration depth μ_1, the heat diffuses into the material and the surface of the part responds in a predictable way to the applied heat source. As a rule of thumb, defects that are present at two times the penetration depth can be detected. Since μ_1 is small, only defects close to the surface can be detected. Situation 2 is the case where the modulation frequency f_2 is lower than f_1. Since the frequency of the modulation is decreased, the penetration depth is increased, see Figure 4.6 situation 2. When the modulation frequency is further reduced, the penetration depth can become larger than the thickness of the part, visualised in Figure 4.6 as situation 3. In situation 3, where the penetration depth μ_3 is larger than the thickness of the part, more than the entire thickness is inspected and generally the detectability of the defects will be reduced. care should be taken with thin walled constructions Therefore, care should be taken with choosing the modulation frequency *f*, especially for the thin walled constructions.

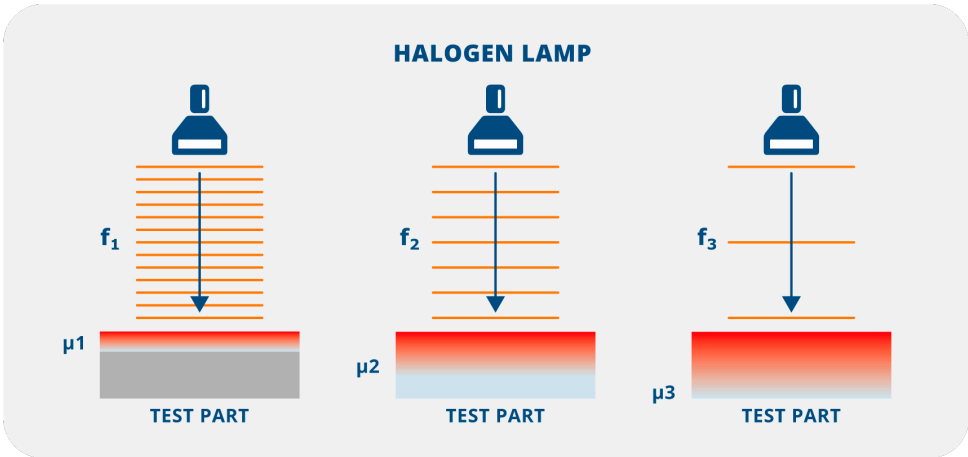

Figure 4.6: Schematic diffusion length μ at different modulation frequencies f, [6]

The thermal wave induced by the excitation will travel inside the material until it is dampened or it will be reflected when an interface is reached. The reflection coefficient *R* can be calculated with the following formula:

$$R_{12} = \frac{e_1 - e_2}{e_1 + e_2} \tag{4.7}$$

where R_{12} is the reflection coefficient between material 1 and 2 and e_1 and e_2 are the thermal effusivity values of material 1 and 2, respectively.

When e_1 and e_2 are equal values, no reflection will take place. When the difference between e_1 and e_2 is small, only a small portion of the wave will be reflected. When the difference is large, almost the entire wave is reflected at the interface. Therefore, the difference in effusivity between sound material and defect material must be large enough to cause reflection at the interface, leading to a contrast difference in the phase images.

The thermal waves reflected by an interface will interact and change the sinusoidal temperature wave created by the halogen lamps, leading to change in amplitude and phase. For each pixel of the image obtained by the IR-camera, the amplitude (A) and phase (φ) of the surface temperature of the test part with respect to the excitation signal is calculated. Figure 4.7 shows the principle of phase and amplitude calculation (four-points method) between the input thermal signal of the halogen lamps and the reflected thermal response signal from the material under test. The points S_1 to S_4 are evenly divided over one period. The phase and amplitude can be calculated using the following formula's [7].

$$\text{Phase } \varphi = atan\frac{S1 - S3}{S2 - S4} \tag{4.8}$$

$$\text{Amplitude } A = \sqrt{S1 - S3^2 + S2 - S4^2} \tag{4.9}$$

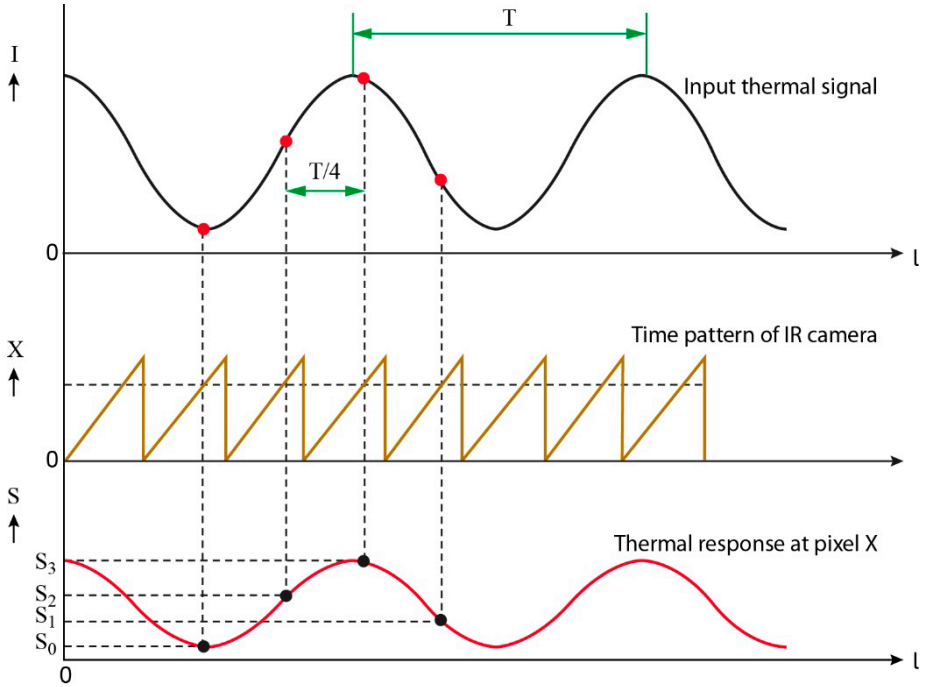

Figure 4.7: Principle of phase and amplitude calculations of OLT [7]

When an interface is present in the material, the phase and amplitude will be different as compared to material that does not have this interfaces. Based on the above mentioned principle, it is necessary to have both defect-free pixel data and defect pixel data in one data set, or to have a calibrated reference. The four-point method is used as an example, normally the phase and amplitude are extracted using a Discrete Fourier Transform (DFT) at the modulation frequency. To reconstruct a proper phase image with acceptable noise, the amplitude should be sufficient. It is always possible to calculate a phase value, but with too low amplitude signals, the noise will be too great. In the amplitude image, different surface conditions, non-uniform heating and background reflections will influence the result of the IRT measurement. The main advantage of the phase image is that it is less affected by these conditions, leading to a clearer image compared to the amplitude image. All OLT thermography images shown in this report are phase images at specific frequencies

4.4 Pulse Thermography

Pulse Thermography (PT) consists of heating up the component under test with a heating pulse of relatively short duration (<< 1 sec) to create a disrupted thermal balance, see Figure 4.8. This disturbance propagates into the material by heat conduction. Before the inspection, the component must be in a steady condition (thermal equilibrium). Heating is generally performed with powerful xenon flash lamps. The high-end xenon flash lamps and the special generator to generate a short burst signal make the equipment more expensive in comparison to lock-in thermography. Furthermore, safety measures must be in place because the xenon flash lamps may cause serious eye injuries. This technique has a limited depth range and is therefore most suitable for the fast inspection of relatively thin specimens. The area of inspection is generally smaller compared to lock-in thermography.

When the heat pulse duration is long (> 1 sec), then this pulse thermography method is called Long Pulse Thermography (LPT), sometimes referred as transient thermography. In case of LPT, heating can also be accomplished with halogen lamps. This technique provides a maximum penetration depth in the test part. To create a thermal imbalance, also cooling of an object can be used [1, 5].

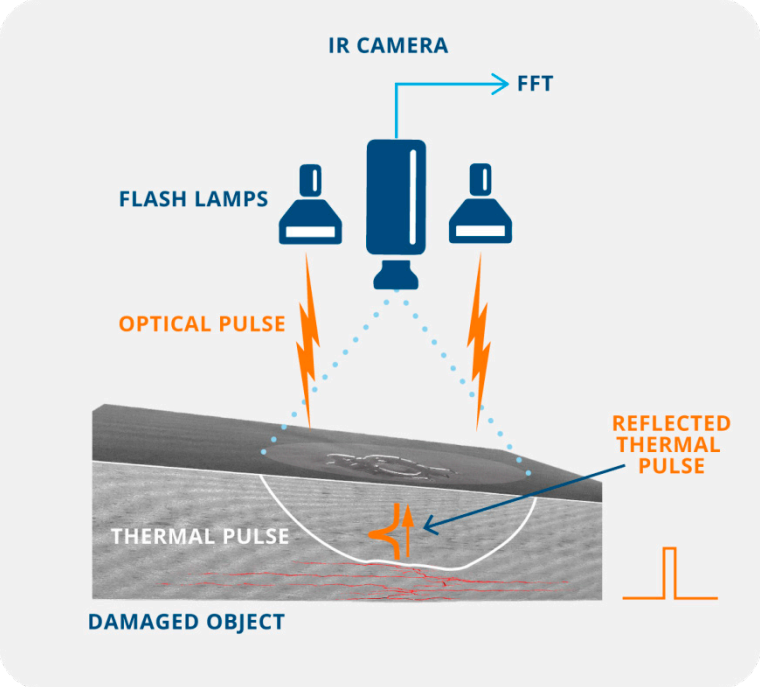

Figure 4.8: Principle of Pulse Thermography (PT)

An infrared camera monitors the temperature variation of the inspected surface. The temperature of the part first increases due to the heat pulse. Increase of temperature will decay over time due to heat being conducted into the part. Sub-surface defects reduce the conduction of heat away from the surface and therefore reduce the surface cooling rate compared to that occurring over non-defective regions. From the time-domain response, this disturbance will be visible. However, the data can also be analysed in the frequency domain. A DFT is applied for every pixel which gives amplitude and phase information at different frequencies. Higher frequencies will contain defects close to the surface and lower frequencies will contain deeper defects. All pulse thermography images shown in this report are phase images at specific frequencies. The Field Of View (FOV) of an infrared camera is about 1 m^2. A homogenous heating will improve the inspection results. There is always an optimum; applied heat energy by the lamps, homogenous heating, chosen FOV, camera settings and evaluation frequencies.

4.5 Analysing Thermography Data

As mentioned in previous sections, the phase images will be less affected by different surface conditions, non-uniform heating and background reflections. Therefore, the final analysis for standard NDI applications is performed using the phase data.

Determination of the Signal to Noise Ratio (SNR):
The detectability of a defect is the first requirement for a successful NDI inspection. When analysing phase images with the human eye, the assessment of the data is more or less subjective. To get a more consistent end results, it is possible to measure the signal to Noise Ratio (SNR) between sound material (close to the defect location) and the defect itself.

- The noise is calculated as the standard deviation from the sound material area.
- The signal is the calculated difference between the mean value of the defect area and the mean value of the sound material area.
- SNR = signal/noise.

There are some practical restrictions in measuring the SNR:

- In a phase image, there is a distortion at the edges of the component (edge effect). When a defect is in close proximity of an edge (or structural part e.g. stiffener), care must be taken in selecting the sound material reference area.
- Impact damage in composite material mostly consists of multilayer delaminations. Due to the multiple reflections of the thermal wave multiple phase angles are measured in the defect area. The mean value of these different phase angles can lead to a lower SNR. Theoretically, the defect mean value can correspond to the selected sound material mean value, the SNR than suggests no defect, but interpretation with the human eye clearly sees the defect based on the phase angle jumps at the defect area.

Blind frequency:
To detect a defect there must be phase difference between the defect area and the sound material area. Depending on the depth and type of defect, this phase difference between the defect and base material become (almost) zero in certain modulation frequency. This frequency is called blind frequency. Figure 4.9 shows the blind frequency of Teflon foil T3;1 of composite reference panel A2, indicated at the red circle (simulated result, [8]). A practical work range of the modulation frequency for inspecting composite material is 0.5Hz to 0.005 Hz. At this frequency range the blind frequency will not occur. Notice that, at a lower frequency, there is also 0 degrees phase difference between sound material and a defect (blue circle), see Figure 4.9. This point is the so-called phase transition frequency. It can be seen that in the working frequency range the largest phase differences can be expected. It is convenient to have a phase transition frequency (blue circle) in the acquired test results because it gives additional information w.r.t. defect characterisation.

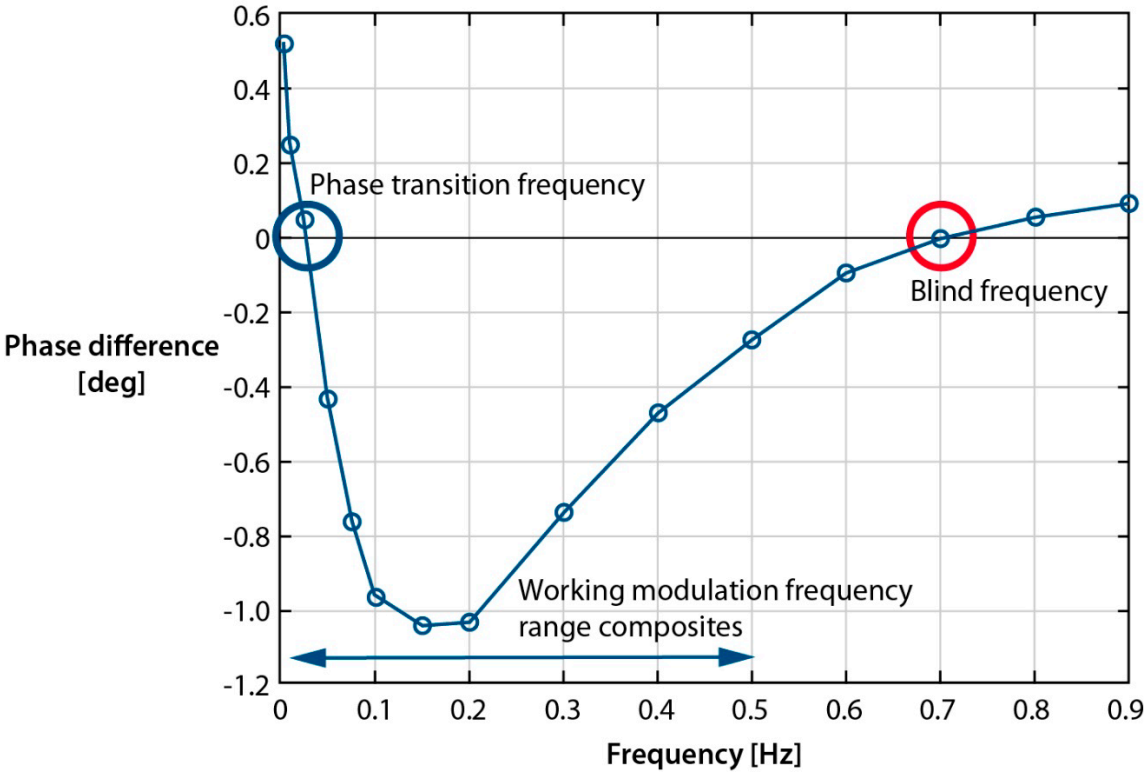

Figure 4.9: Phase difference between defective and non-defective area as a function of the excitation frequency with highlighted blind frequency f_b (simulated for NTP-A2 panel defect T3;1)

Practical sizing of defects:

When defects are detected, sizing in planar direction can be performed. In some extend, it is also possible to perform a depth estimation (not investigated in this program). For correct sizing, the pixels of the phase image must be calibrated using well defined markers in the phase image. Figure 4.10 shows a red line between two known markers. By calibrating the pixel size to the known reference, the damage size can be determined, see Figure 4.11.

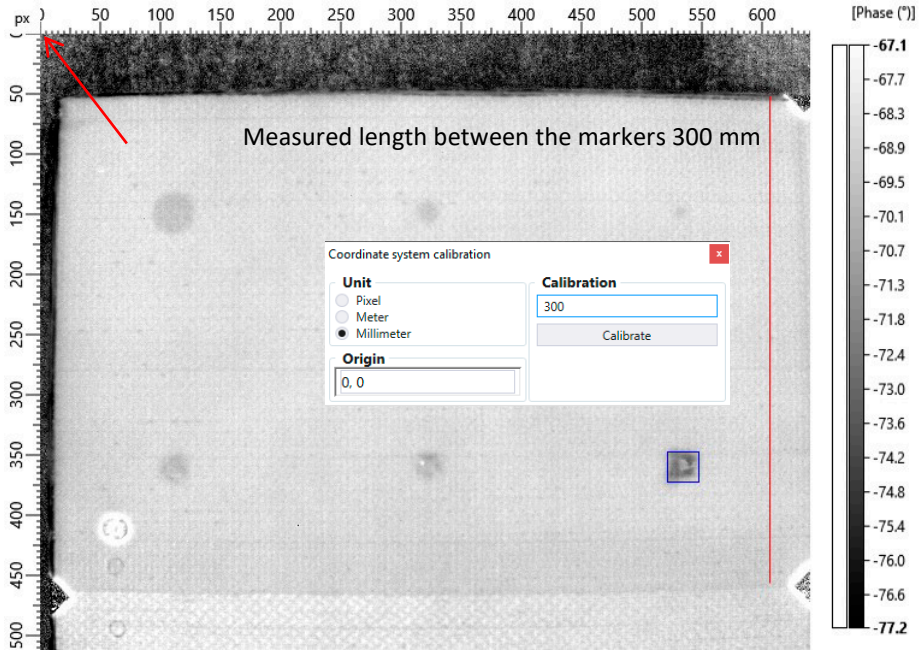

Figure 4.10: Calibrating from pixels to scaled mm

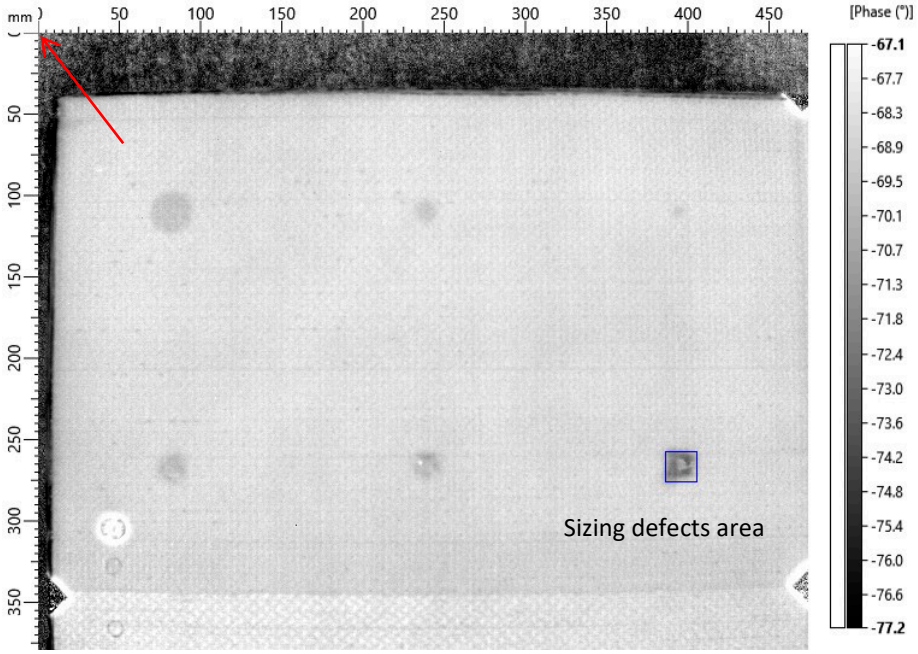

Figure 4.11: Phase image calibrated in mm for correct sizing measurements

4.6 Equipment screening

Apart from different excitation and signal processing methods, the specification of the infrared camera has a significant influence on the inspection results. Modern cameras contain solid state focal plane arrays; a lens will focus incident radiation onto the detector, see Figure 4.12

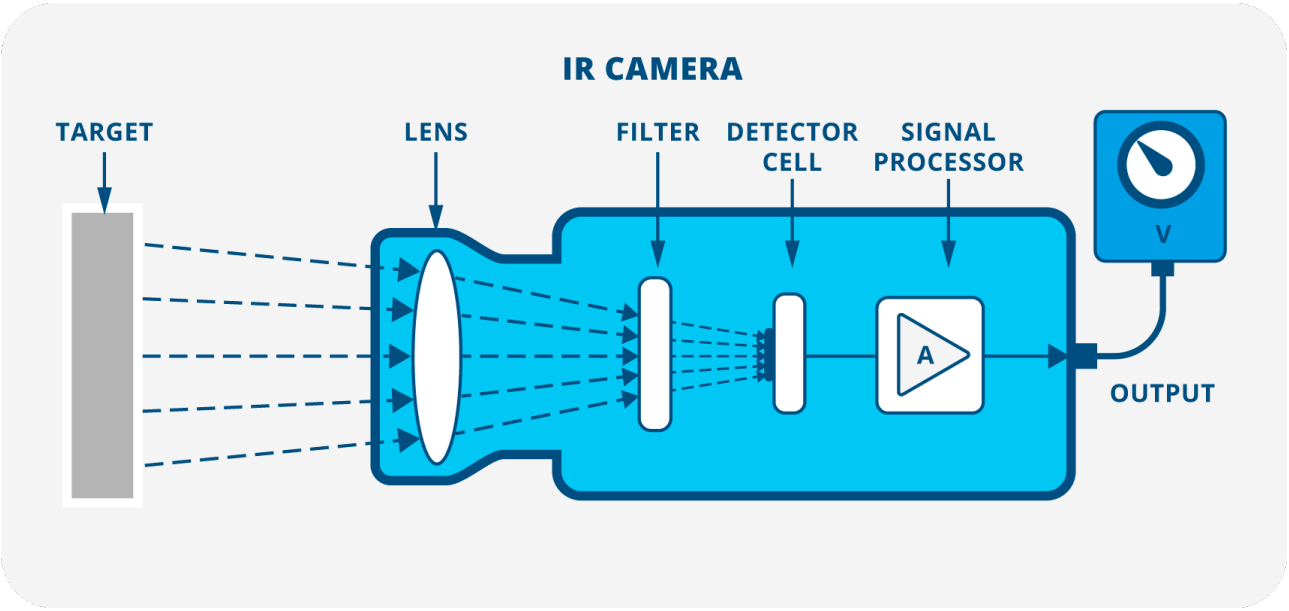

Figure 4.12: Operating principle of an IR camera

IR cameras suited for active thermography operate in the electromagnetic spectrum range from 2 to 5 µm (MWIR) or 8 to 14 µm (long wave). Two types of detectors can be discriminated; quantum detectors which directly detect incident photons or microbolometers which detect changes in thermo-physical properties of a small mass.

The quantum detectors (InSb) are significantly more sensitive and have a faster response than IR camera's with a microbolometer. The quantum detectors operate mostly in the electromagnetic spectrum range from 2 to 5 µm. The quantum detectors are forced cooled, usually by a Stirling cooler. A Stirling cooler is able to cooldown the internal detector to cryogen conditions at 77 K. This is accomplished using liquid nitrogen (boiling point 77 K), resulting in a constant temperature which provides a good sensitivity and less influence of stray radiation from the internal components of the IR camera. The typical Noise Equivalent Temperature Difference (NETD), the minimal temperature difference that can be noticed above noise, is less than 20 mK. Although cooled IR cameras are most effective, there are some disadvantages; the cooled cameras are quite expensive, the Stirling cooler contain rotating parts resulting in an operational life of about 8000 to 12000 hours and cooling down to 77K takes about 15 minutes.

Uncooled cameras using the microbolometer are significantly cheaper and operate mostly in the electromagnetic spectrum range from 8 to 14 µm. The signal to noise performance of these cameras (NETD < 50 mK) is lower compared to a quantum detector. The advantages of uncooled cameras are; cheaper, no cooldown time required and lighter. Further, other specification have an influence on the inspection results and should be considered when selecting a camera; array size (resolution), frame rate, noise equivalent temperature difference and focal optics.

The selection of the optimum camera is primarily based on each applications. The choice of IR camera depends on what sensitivity and spatial resolution are required. Furthermore, other specifications have influence on the inspection results and should be considered when selecting a camera; array size (resolution), frame rate, noise equivalent temperature difference and focal optics. In addition to that, costs, robustness, size/weight of the camera play a role.

5 Thermography Test Results

Infrared thermography inspection of reference specimens A2 and C were carried out by the company Edevis GmbH, located in Stuttgart (Germany). The inspections were closely directed, observed and monitored by the NLR.

5.1 Optical Lock-in thermography

The laboratory set-up to inspect both reference specimens can be seen in Figure 5.1. The inspections were performed from the front side (cupper mesh side) which is most realistic for in-service conditions. The monolithic panel was also inspected from the rear side; one set of foil locations is at a different depth in this situation. The distance of the camera determines the FOV. During the inspections, ¼ of the total surface area of the reference specimen was covered, resulting in an approximately field of view of 450x300 mm. The IR camera uses an 640 x 512 pixel detector in combination with the selected FOV. This results in a resolution about 0.7 mm/px. It is possible to increase the camera/specimen distance and to cover the total surface area during one acquisition, resulting in a decrease of resolution. The position of the lamps is chosen such that a homogeneous heat could be established on the specimen. Furthermore, the angle of the lamps were set such that no disturbing reflection signals could enter the lens of the IR camera.

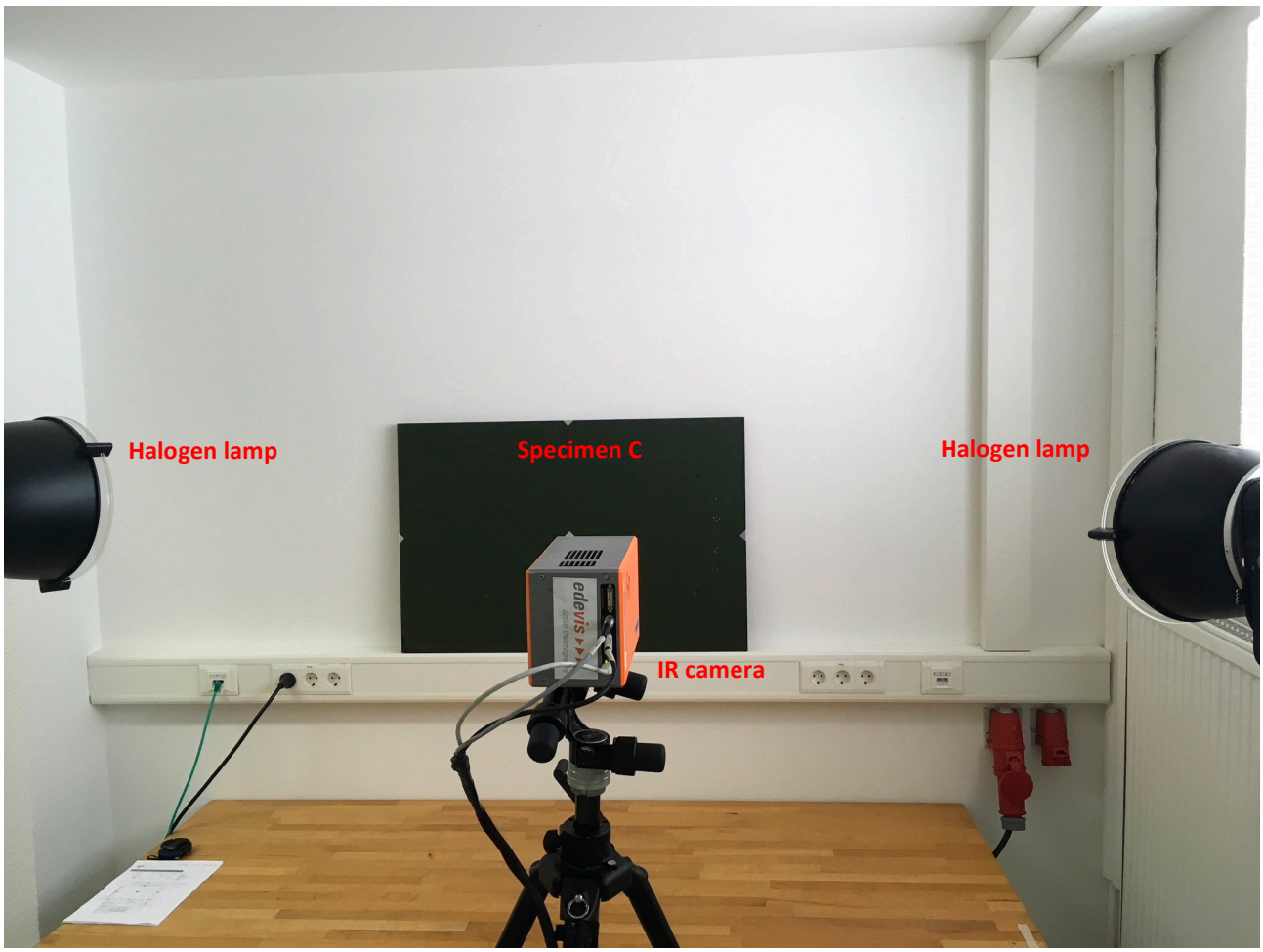

Figure 5.1: OLT thermography inspection of reference specimen C by Edevis GmbH

The laboratory Edevis set-up includes:

IR camera:	IRcam Equus 327kM
Spectral responsivity:	1.5-5.0 µm (Filter LP 4.08 µm)
Detector:	InSb 640 x 512 Pixel
NETD:	< 20 mK @ 30°C
Max. Frame rate:	100 Hz in full frame mode
Applied frame rate:	100 Hz in full frame mode
Integration time:	1200 µs
Lens:	25 mm, F/2
Field of view:	21.7 °H x 17.5°V
Dimmer pack:	Edevis OTvis 12000, max.12 kW Lamps: 2x halogen lamps each with 2kW -> applied power 4 kW max.
Software:	Edevis DisplayIMG 6.2.5.09 – Modul OTvis

5.1.1 Reference Specimen A2

An Optical Lock-in Thermography (OLT) inspection is performed on the complete reference specimen A2. For the complete measurement report, the reader is referred to [9]. In this investigation, the Region Of Inspection (ROI) is ¼ of the total surface area respectively coded with A1 to A4, see Figure 5.2

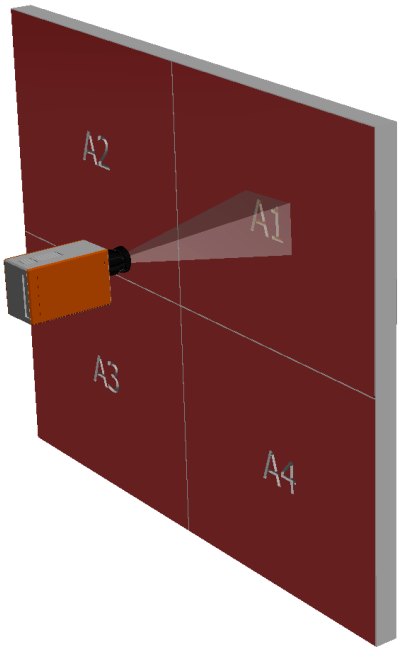

Figure 5.2: Defined inspection areas of reference specimen A2, respectively coded with A1 to A4

For the optical lock-in inspections six modulation frequencies are applied to collect the data. Table 5-1 shows the applied excitation parameters:

- Modulation (Lock-in) frequency of the halogen lamps;
- The maximum power applied to the halogen lamps;
- Conditioning periods are the amount of modulation cycles to pre-heat the specimen (no data collected);
- Acquisition periods are the amount of modulation cycles applied and the data is acquired.

Table 5-1: Applied excitation parameters

Applied excitation parameters				Calculated penetration depth
Lock-in frequency [Hz]	**Power max [kW]**	**Conditioning periods**	**Acquisition periods**	**Penetration depth (mm) @ 4.16e-7 (m^2/s)**
0.5	3.8	3	8	0.51
0.2	3.8	3	5	0.81
0.1	3.2	1	3	1.15
0.05	2.8	0	2	1.63
0.01	2.6	0	1	3.64
0.005	2.4	0	1	5.15

Figure 5.3 shows the influence of the modulation frequency on the test results for inspection area A2. This inspection area A2 includes the impacts $*^{1.20}$, $+^{3.20}$ and $+^{5.40}$, the foil locations T1,1,c , T2,1,c and T3,1,c. At the highest frequency (0.5 Hz), the damage caused by the impact is sharply represented in the phase images. However, the foil locations at a depth of 0.7 mm could not be detected in the same images. At 0.2 Hz, the fabric of the composite fibres are more presented in the phase image (0, 90 and +/- 45 degrees). Furthermore, the damaged surface area of the impact locations is extended compared to the 0.5 Hz test results. Additionally, the three foil locations at a depth of 0.7 mm are now clearly visible. At 0.1 Hz, all defects are visible but with a lower SNR compared to the test results obtained with 0.2 Hz. At 0.05 Hz, only the impact damages are visible; the foil locations cannot be detected anymore. This is most likely caused by the phased transmission frequency. At the phase images of 0.01 and 0.005 Hz, the foil locations can hardly be seen and the impact locations are well detected. Interestingly, the defect locations are indicated in white at these frequencies instead of black as with the frequencies 0.5, 0.2 and 0.1Hz. The phase shift is between 0.1 and 0.05 Hz which indicates that this frequency is close to the so-called phase transition frequency.

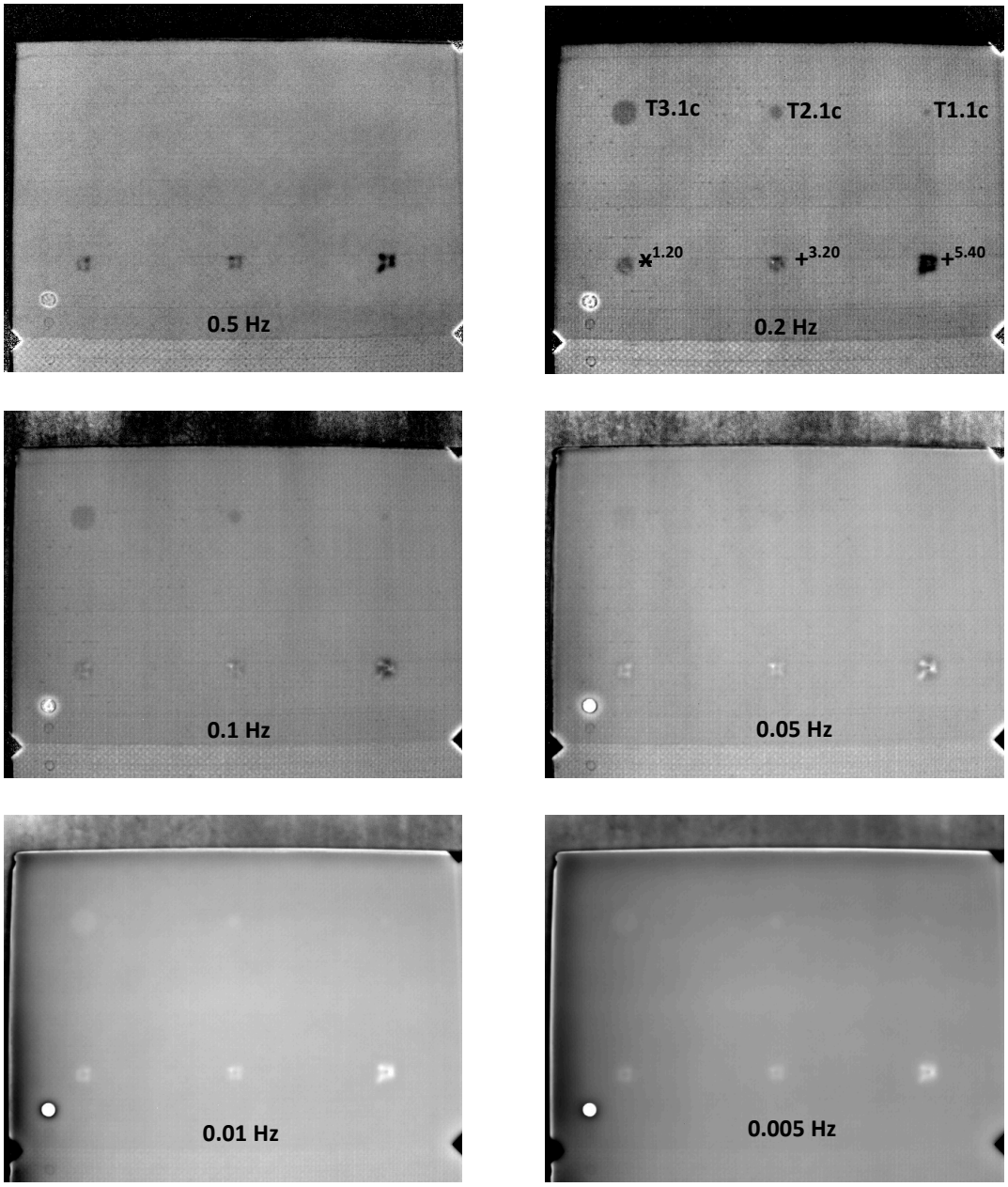

Figure 5.3: Influence of the modulation frequency on the phase images, inspection area A-A2

Remark: The defect signal of the impact damage, which is clearly visible in the phase image, is caused by multilayer delamination and fibre breakages. Multiple reflections between these boundaries lead to phase angle jumps, which in turn can have a significant effect on the mean value of the phase angle. In the worst case, the mean value of the defective area corresponds exactly to that of the intact material [9].Therefore, multi-frequency approach is recommended.

The foil locations at depths at 3.4 and 4.7 mm are not detected with OLT, when the panel is inspected from the rear side the foil locations T1.2c, T2.2c, T3.2c, T1.2, T2.2 and T3.2 are positioned at a depth at 2 mm. But also at this depth the OLT technique is not capable to detect the foils. Figure 5.4 shows the position of the foils at a depth of 2 mm (yellow dashed rectangles).

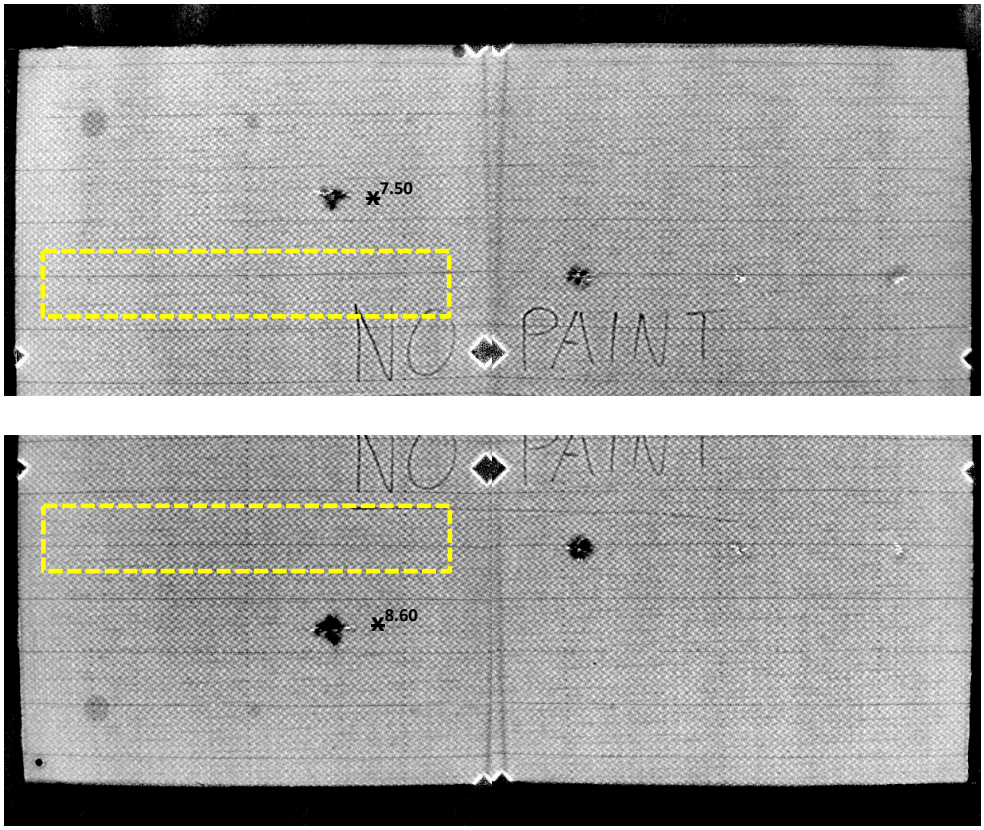

Figure 5.4: Phase image of 0.2 Hz, inspected from rear side covering the entire specimen. Yellow dashed rectangles indicate area where foils are inserted at 2 mm depth

Figure 5.5 shows the influence of the modulation frequency on the test results for the complete specimen. The following general observations of reference specimen A2 can be made:

- All impact locations are detected. No significant influence can be observed w.r.t. detectability between the different applied frequencies. The delaminations have somewhat cloverleaf shape. Based on visual appearance, the 0.2 Hz modulation frequency shows for e.g. impact location $+^{5.40}$ the most uniform representation of the damaged surface area, other frequencies show a more intermittent pattern.
- Foil locations with diameters of ¼, ½ and 1 inch diameter at a depth of 0.7 mm are detected.
- Foil locations at a depth 2.0, 3.4 and 4.7 mm are not detected.
- No significant differences between the test results with and without copper mesh can be seen.

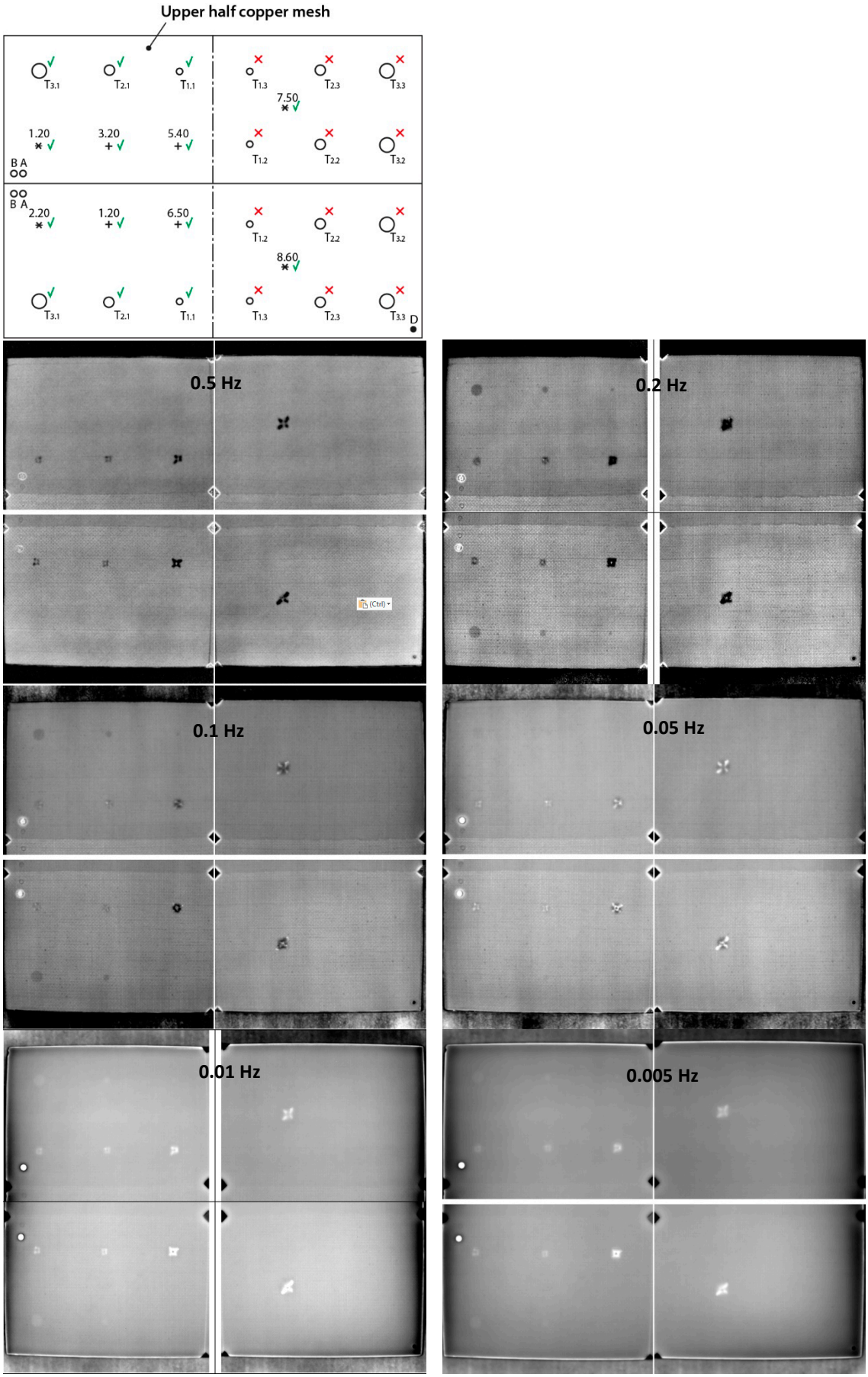

Figure 5.5: Influence of the modulation frequency on the phase images, complete specimen A2

Table 5-2 shows a summary of the test results on the test specimen A2. When a defect is detected, a SNR value is determined. Furthermore, the actual sizes of the artificial defects are provided, which can be compared to the measured sizes of the detected defects acquired by thermography. To determine the detectability and sizing capability of the thermography method w.r.t. real impact delamination, ultrasonic data is used as a reference, see for example Figure 5.6.

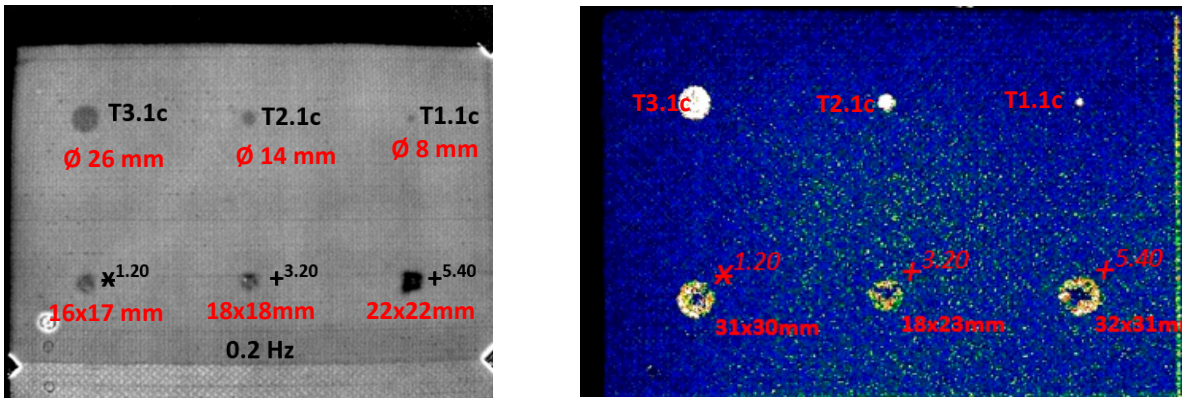

Figure 5.6: Phase image 0.2 Hz and ultrasonic pulse-echo reflection C-scan test results

Table 5-2: Measured Signal-to-Noise Ratio and sizing of defects of reference specimen A2 using optical Lock-in thermography

Reference specimen A2			Optical Lock-in thermography (OLT)											
	Defect type	Actual size	SNR						Measured size w/h [mm] @ corresponding frequency [Hz]					
		Dia./ depth [mm]	0.5	0.2	0.1	0.05	0.01	0.005	0.5	0.2	0.1	0.05	0.01	0.005
With copper mesh	T1,1,c	6.35/0.7		2.4	3.2		1.4	0.8		8	8	8		
	T2,1,c	12.7/0.7		3.5	3.8		1.7	1.2		14	14	14		
	T3,1,c	25.4/0.7		4.3	4.4	4.9	3.1	3.5		26	26	26		
	T1,2,c	6.35/3.4												
	T2,2,c	12.7/3.4												
	T3,2,c	25.4/3.4												
	T1,3,c	6.35/4.7												
	T2,3,c	12.7/4.7												
	T3,3,c	25.4/4.7												
	*1.20	31x30	3.6	5.0	3.7	2.3	5.0	6.6	15x16	16x17	16x17	16x17	14x17	12x16
	+3.20	18x23	5.1	5.2	1.1	2.7	7.1	6.8	14x16	18x18	22x19	20x7	18x14	18x14
	+5.40	32x31	9.6	13.3	9.6	0.3	11.7	13.1	22x20	22x22	24x26	24x26	19x23	18x19
	*7.50	42x38	6.1	7.9	3.4	1.4	8.7	10.3	29x33	27x30	28x31	30x32	26x30	26x30
Without copper mesh	T1,1	6.35/0.7		0.6	1.2					8	8			
	T2,1	12.7/0.7		1.3	1.5		2.0	2.8		13	13			
	T3,1	25.4/0.7		2.5	3.1		5.5	7.3		26	26		26	
	T1,2	6.35/3.4												
	T2,2	12.7/3.4												
	T3,2	25.4/3.4												
	T1.3	6.35/4.7												
	T2.3	12.7/4.7												
	T3.3	25.4/4.7												
	*2.20	31x29	3.7	4.0	0.9	0.0	0.3	0.0	17x18	17x18	17x18	17x18	17x18	15x17
	+4,20	21x27	3.5	3.8	0.8	1.4	6.0	6.9	18x19	18x19	18x19	15x16	15x16	15x16
	+6.50	37x29	12.8	16.9	9.6	0.3	19	19.9	25x24	25x20	24x22	26x24	27x23	23x20
	*8.60	42x40	7.1	9.1	6.3	1.0	11.2	16.0	33x32	33x32	33x32	33x32	33x32	33x32

The following general observations are made w.r.t. the sizing ability of the thermography method:

- ***Sizing ability foils:***

Considering the measured defect size with OLT, the foils at 0.7 mm depth are slightly oversized within 2 mm, compared to the actual diameters of the foils. The estimation of defect size is performed with the pixel calibration procedure, see Section 4.5. Considering that this estimation is based on the calibrated results, the defect sizing seems to be reasonably good.

- ***Sizing ability Impacts:***

On the other hand, the estimation of impact damages are significantly undersized compared to the ultrasonic pulse-echo data of Figure 3.3. For example, at impact location $*^{1.20}$, the damage detection by the OLT is underestimating with almost a factor 2. Because of the multilayer delamination, the OLT has detected most probably the upper part of the delamination only.

5.1.2 Reference specimen C

An OLT inspection is performed on the complete reference specimen C, see [9]. In this investigation the Region Of Inspection (ROI) is ¼ of the total surface area respectively coded with A1 to A4, see Figure 5.7

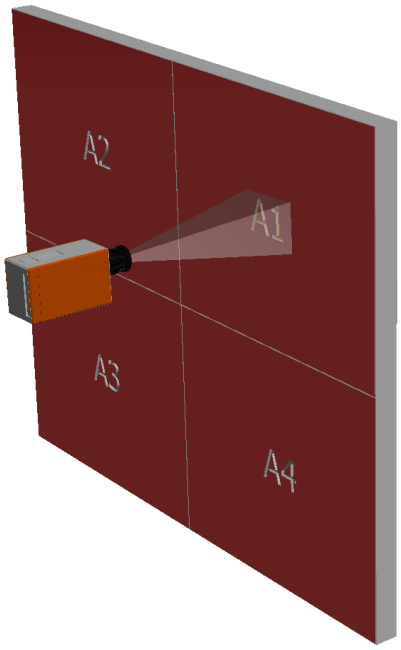

Figure 5.7: Defined inspection areas of reference specimen C, respectively coded with C-A1 to C-A4

For the OLT inspections, six modulation frequencies are applied to collect the data, identically to the frequencies used for the specimen A2. Table 5-3 shows the applied excitation parameters.

Table 5-3: Applied excitation parameters

Applied excitation parameters				Calculated penetration depth
Lock-in frequency [Hz]	Power max [kW]	Conditioning periods	Acquisition periods	Penetration depth (mm) @ 4.16e-7 (m^2/s)
0.5	3.8	3	8	0.51
0.2	3.8	3	5	0.81
0.1	3.2	1	3	1.15
0.05	2.8	0	2	1.63
0.01	2.6	0	1	3.64
0.005	2.4	0	1	5.15

Figure 5.8 shows the influence of the modulation frequency on the test results for inspection area C-A2. Inspection area C-A2 includes the impact $+^{1.20}$, foil locations T1,1,c , T2,1,c and T3,1,c, skin-to-honeycomb core disbonds HD2, HD3 and HD4 and water ingress in the Nomex honeycomb cells W1, W4 and W5. At the highest frequency (0.5 Hz), the damage caused by the impact is sharply represented in the phase images. However, all other artificial defects could not be detected. At 0.2 Hz, no significant differences in test results compared to the phase image of 0.5 Hz could be observed. Only the water ingress locations are slightly visible. At 0.1 Hz, the foil locations T2.1c and T3.1c with respectively diameters of ½ and 1 inch at a depth of 1.5 mm could be detected. Furthermore, the water ingress locations W4 and W5 are slightly more visible compared to the 0.5 Hz phase images. At 0.05 Hz, the detectability of all artificial defects is reduced. At the frequency of 0.01 Hz, the skin-to-honeycomb core disbonds HD3 and HD4 can be detected and also the water ingress locations W4 and W5 are clearly visible. On the other hand, the foil locations T2.1c and T3.1c could not be detected anymore at this frequency. This is an indication of the phase transitions frequency. At the frequency 0.05 Hz, only the water ingress W4 and W5 and impact location $+^{1.20}$ are visible. All other artificial defects could not be indicated.

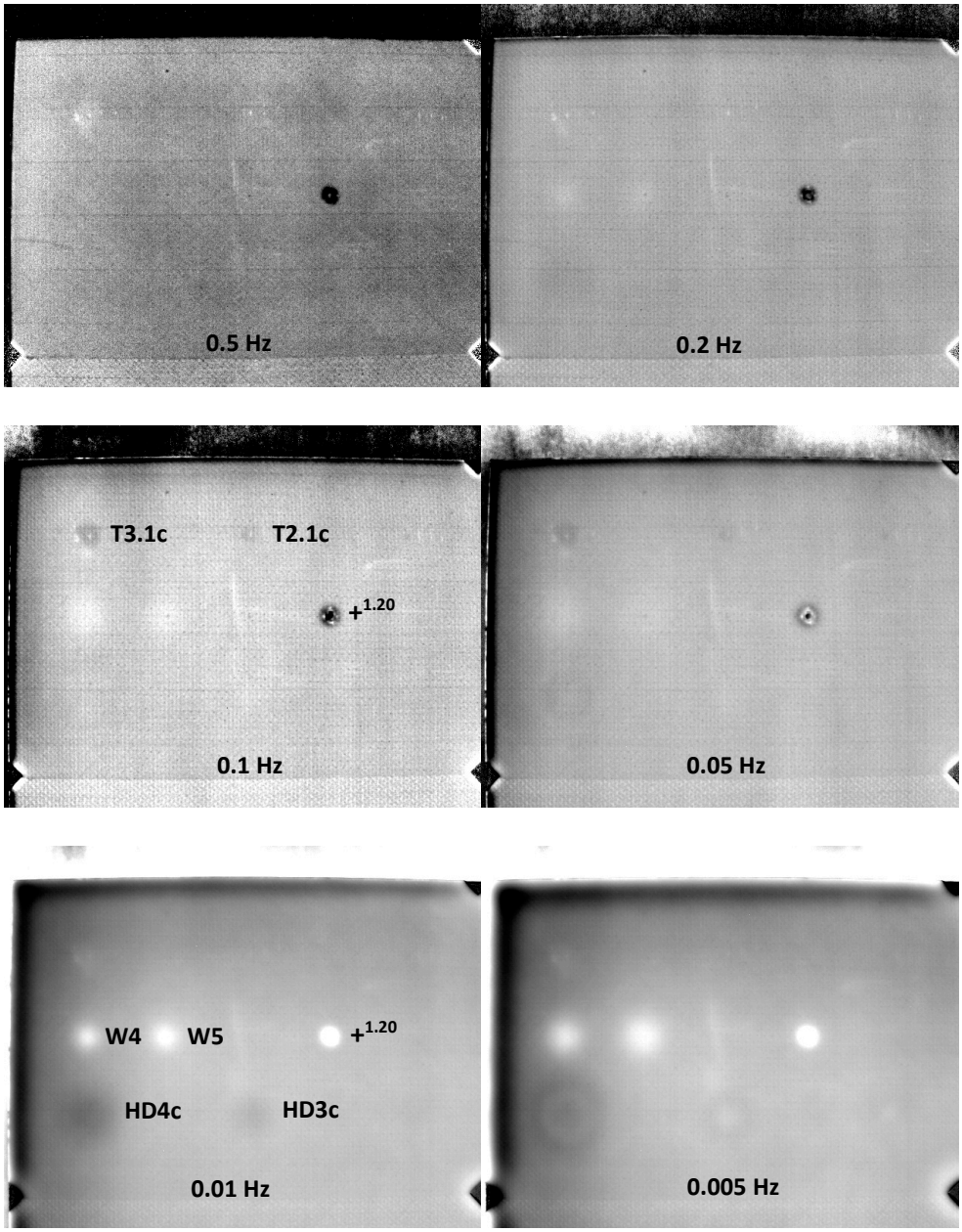

Figure 5.8: Influence of the modulation frequency on the phase images, inspection area C-A2

Figure 5.9 shows the influence of the modulation frequency on the test results for the complete specimen.
The following general observations of reference specimen C can be made:

- All impact locations could be detected. No significant influence could be observed w.r.t. detectability between the different applied frequencies.
- Foil locations of a ½ and 1 inch are detected at a depth of 1.5 mm at frequencies of 0.1 and 0.05 Hz, both with and without copper mesh.
- Foil location T3.2 with 1 inch diameter and at a depth of 2.25 mm is detected at a frequency of 0.05Hz, however, the SNR of this measurement was relatively low. Moreover, other foil locations at a depth of 2.25 mm could not be detected.
- Skin-to-honeycomb core disbonds of a ½, 1 and 2 inch diameter at the depth of 3 mm were successfully detected. At the modulation frequency of 0.005 Hz, the indication of the disbond has an appearance of multiple circles. The disbonds with a diameter of ¼ inch was not detectable.

- The water ingress in the Nomex honeycomb cells W4 and W5 were successfully detected (7 cells are filled with water). The water ingress location W1 to W3 (1 or 3 cells filled with water) could not be detected. Remark: The filling of the cells with water was performed in 2015 [10]. Due to possible diffusion of the water through the Nomex cells, the artificial water ingress defects should be treated as unreliable. Although W4 and W5 were detected, no further analysis is be performed.
- No significant differences were observed between the test results with and without copper mesh.
- Phase transition frequency for impact damage is observed between the modulation frequencies 0.05 and 0.01 Hz, evident at impact location $+^{1.20}$.

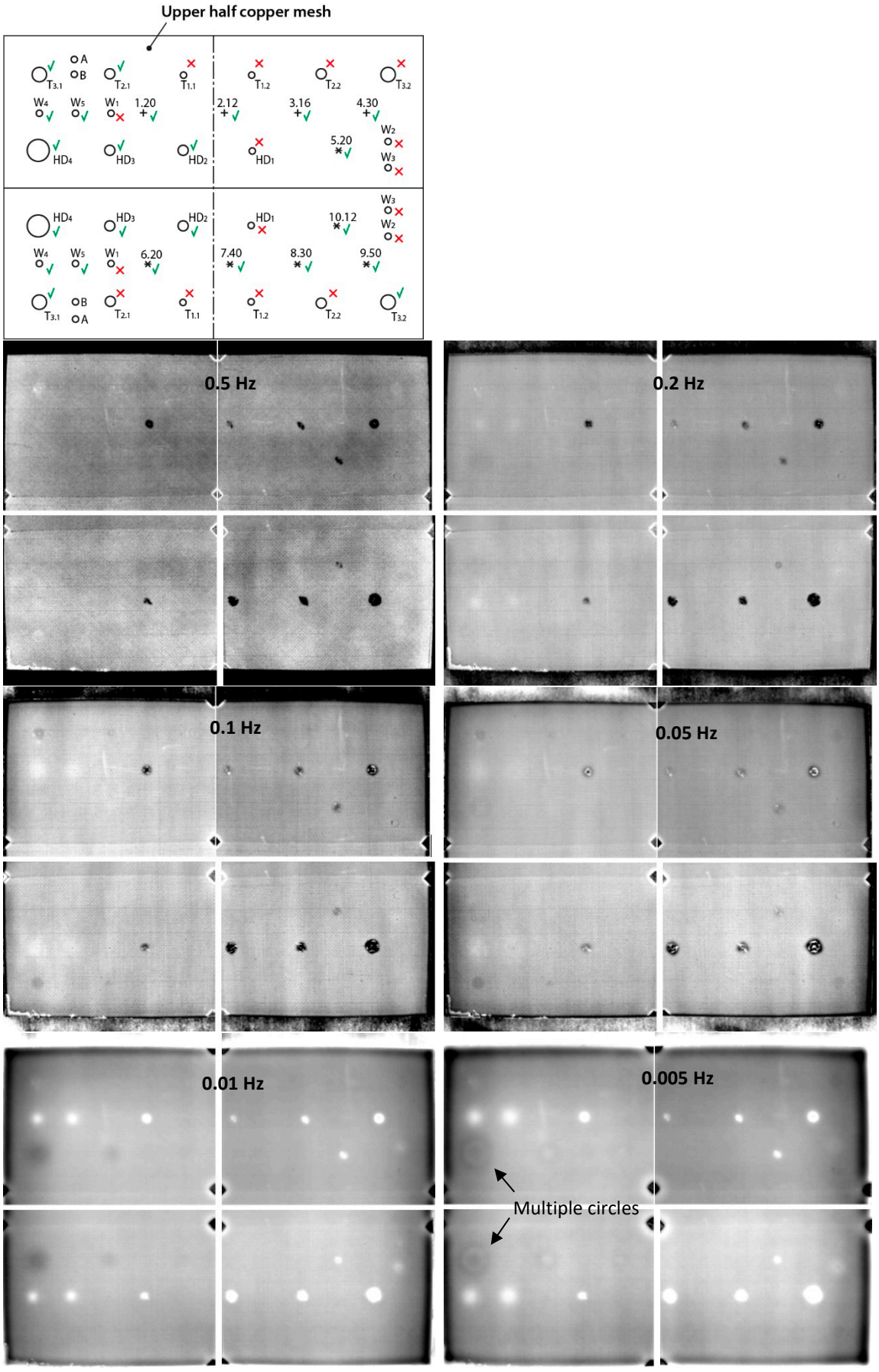

Figure 5.9: Influence of the modulation frequency on the phase images, complete specimen C

When a defect is detected, a SNR value is determined. Furthermore, the actual sizes of the artificial defects are provided, which can be compared to the measured sizes of the detected defects acquired by thermography.
To determine the detectability and sizing capability of the thermography method w.r.t. real impact delamination, ultrasonic data is used as a reference, see for example Figure 5.10.

Table 5-4 shows an overview of the SNR of all artificial locations. In principle, the higher the SNR, the better the defect location is presented in the phase image. Comparable to the test results of reference panel A2, there is no single frequency that can be assigned as optimum frequency to inspect this sandwich panel based on SNR. Table 5-4 does not show an overview of the water ingress honeycomb cells. The locations W4 and W5 comprise the fill of 7 cells W4 fully filled and W5 half full filled. The water ingress honeycomb cells are detected at the lower frequencies of 0.01 HZ and 0.005 Hz.

Table 5-4: Measured SNR and sizing of defects of reference specimen C using OLT

Reference specimen C			Optical Lock-in thermography (OLT)											
	Defect type	Actual size	SNR [Hz]						Measured size w/h [mm] @ corresponding frequency [Hz]					
		Dia./ depth [mm]	0.5	0.2	0.1	0.05	0.01	0.005	0.5	0.2	0.1	0.05	0.01	0.005
With copper mesh	T1,1,c	6.35/1.5												
	T2,1,c	12.7/1.5			1.8	2.0					14x14	14x14		
	T3,1,c	25.4/1.5			2.5	4.7					25x25	25x25	-	-
	T1,2,c	6.35/2.25												
	T2,2,c	12.7/2.25												
	T3,2,c	25.4/2.25												
	HD1	6.35/3.0												
	HD2	12.7/3.0												
	HD3	25.4/3.0					1.0	1.2						
	HD4	50.8/3.0		0.9		1.5	9.6	6.2						50x50
	+[1,20]	PE 20x19 TT 54x60	11.1	16.7	12.4	4.8	55.4	68.4	21x20	21x20	22x22	26x25	17x18	18x19
	+[2,12]	PE 17x18 TT 54x57	2.2	2.2	1.6	0.7	7.3	6.9	14x17	14x18	14x18	14x18	14x18	14x18
	+[3,16]	PE 23x20 TT 60x62	6.5	9.2	5.6	1.4	1.3	22.4	17x17	17x17	18x18	18x18	18x18	18x18
	+[4,30]	PE 25x23 TT 64x66	19	30.7	21.2	7.5	36.6	50.6	22x22	22x22	23x23	29x27	19x19	19x19
	*[5,20]	PE 23x21 TT 77x77	6.7	9.8	6.4	4.4	14.6	17.6	17x17	17x17	17x17	18x18	18x18	18x18
Without copper mesh	T1,1	6.35/1.5												
	T2,1	12.7/1.5												
	T3,1	25.4/1.5	0.5		1.5	4.5						27x27		
	T1,2	6.35/2.25												
	T2,2	12.7/2.25												
	T3,2	25.4/2.25				1.0		1.2						26x29
	HD1	6.35/3.0												
	HD2	12.7/3.0					1.1	1.1						
	HD3	25.4/3.0					2.6	1.2						
	HD4	50.8/3.0					9.8	3.5					34x34	
	*[6,20]	PE 26x23 TT 74x72	6.7	8.5	5.1	1.7	22.2	18.6	15x15	16x16	18x18	21x21	21x18	18x17
	*[7,40]	PE 35x36 TT 85x87	11.1	18	14.5	8.5	27.6	39.6	23x22	24x23	28x28	31x31	29x30	32x33
	*[8,30]	PE 33x26 TT 83x77	10.3	13.2	9.3	3.2	23.5	29.7	23x22	22x23	26x25	28x29	30x29	30x29
	*[9,50]	PE 45x41 TT 81x81	16.7	25.4	20.4	9.3	35.6	54	28x27	29x31	32x33	36x36	40x39	43x42
	*[10,12]	PE 20x20 TT 57x55	3.2	3.2	2.3	0.7	8.2	8.8	15x17	15x17	18x17	18x17	19x20	18x19

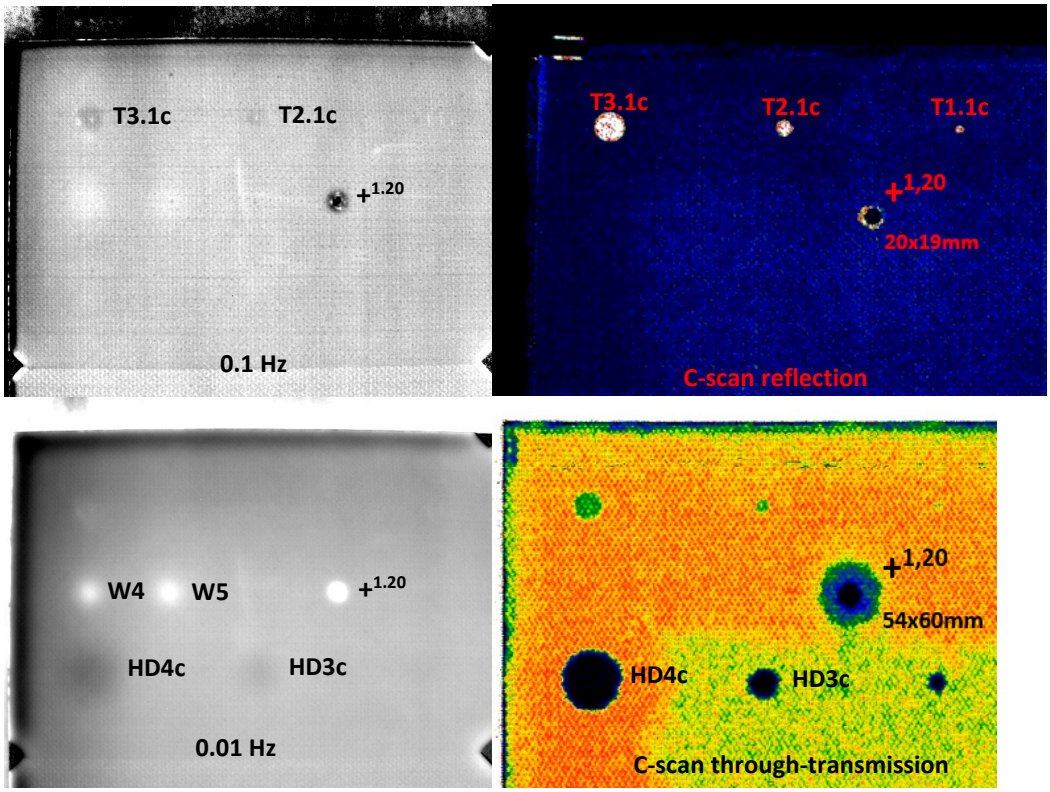

Figure 5.10: Phase image at the frequency of 0.1 Hz and 0.01Hz (left). Ultrasonic pulse-echo reflection and through-transmission C-scan test results are shown on the right hand side. Remark: at the time of acquiring the C-scan data, the water-ingress was not present

The following general observations are made w.r.t. the sizing ability of the thermography method:

- ***Sizing ability foils:***
  The OLT measurements estimated the sizes of the foils at 1.5 and 2.25 mm depth slightly to large but within 2 mm from the nominal size. The estimation of defect size is performed with the pixel calibration procedure, see Section 4.5. Considering that this estimation is based on the calibrated results, the defect sizing seems to be reasonably good.
- ***Sizing ability Impacts:***
  At the impact locations, two type of damages can occur; 1) delamination in the skin, and 2) skin-to-core disbonds. For the delamination area in the skin, the sizing of the thermography data was roughly in line with the ultrasonic pulse-echo C-scan data (max deviation approx. 6 mm). When the sizing of the thermography data is compared to the through-transmission C-scan, the impact damages were significantly undersized by the OLT. Possible cause could be that skin-to-core disbonds around the impact locations are not detected by the OLT. It is noted that the artificial skin to honeycomb disbonds were detectable with OLT (see the next bullet point). On the other hand, the through-transmission C-scan data shows not a complete attenuation of the sound beam at the impact location which is an indication that the core is not completely separated from the skin.
- ***Sizing ability Skin-to-honeycomb core disbonds:***
  The skin-to-honeycomb core disbond HD4 with a nominal diameter of 2 inch could be detected with a good SNR. The measured size of HD4 (2inch) at the modulation frequency 0.005Hz is 50/50 mm (width x height).

5.2 Test Results Pulse Thermography

The laboratory set-up to inspect both reference specimens with Pulse Thermography (PT) can be seen in Figure 5.11. In this case, the inspection was performed from one side which is most realistic for in-service conditions. The distance of the camera was chosen to cover ¼ of the total surface area of the reference specimen, resulting in an approximate field of view of 450 x 300 mm. It is possible to increase the camera/specimen distance and to cover the total surface area during one acquisition. The position of the lamp is chosen, such that the specimen is homogeneously illuminated and that no disturbing reflection signals are reflected into the lens of the IR camera.

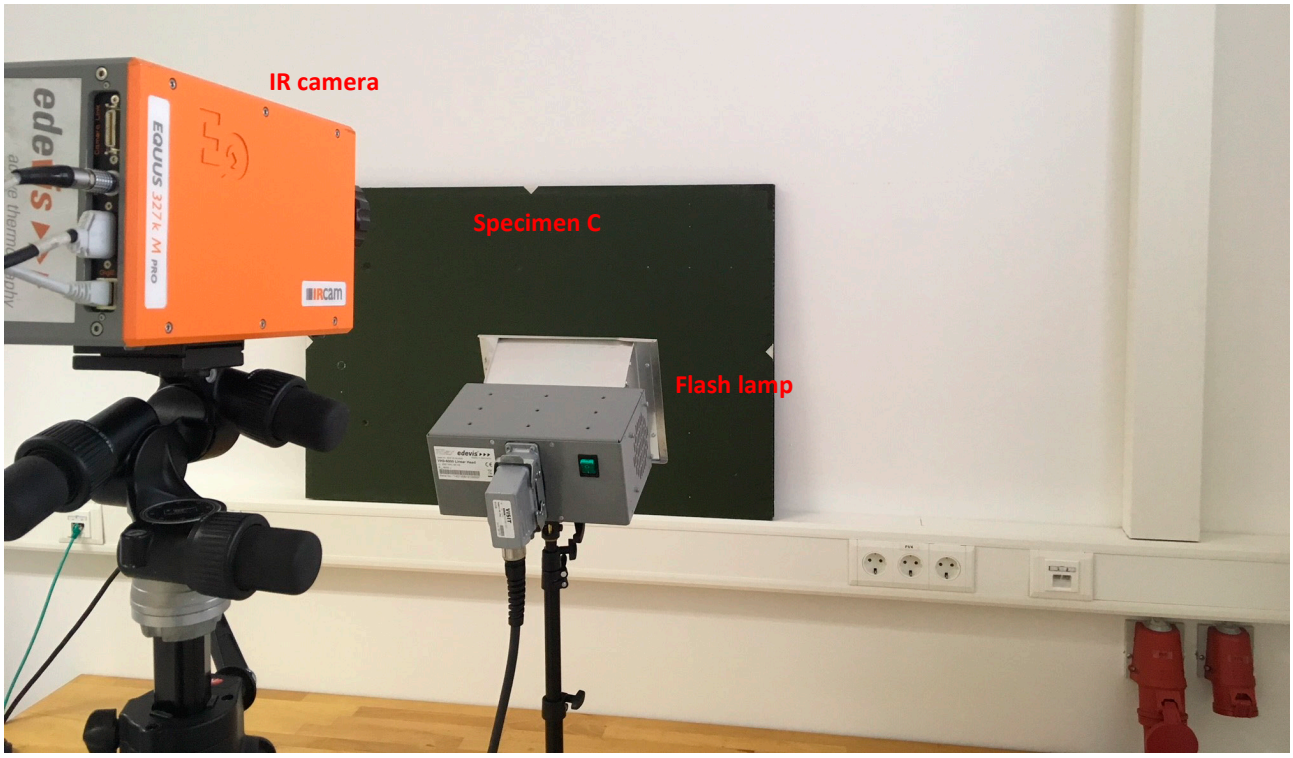

Figure 5.11: PT thermography inspection of reference specimen C by Edevis GmbH

The laboratory Edevis set-up includes:

IR camera:	IRcam Equus 327kM
Spectral responsivity:	1.5-5.0 µm (Filter LP 4.08 µm)
Detector:	InSb 640 x 512 Pixel
NETD:	< 20 mK @ 30°C
Max. Frame rate:	100 Hz in full frame mode
Applied frame rate:	100 Hz in full frame mode
Integration time:	1200 µs
Lens:	25 mm, F/2
Field of view:	21.7 °H x 17.5°V
Flash generator:	Edevis PTvis6000
Flash energy max.:	6 kJ
Lamps:	1 x VH3-6000 Linear Head, max 6kJ
Software:	Edevis DisplayIMG 6.2.5.09 – Modul PTvis

5.2.1 Reference Specimen A2

A PT inspection is performed on the complete reference specimen A2. For the complete measurement report, the reader is referred to [11]. The following parameters are applied:

- Amplitude of flash at 50%.
- Pulse length of 0.01s.
- 10 seconds of recording at 100 Hz.

In this investigation, the ROI is ¼ of the total surface area respectively coded with A1 to A4, see Figure 5.12 In this case, a flash excitation was performed, a heating pulse of relatively short duration (<< 1 sec) to create a disrupted thermal balance.

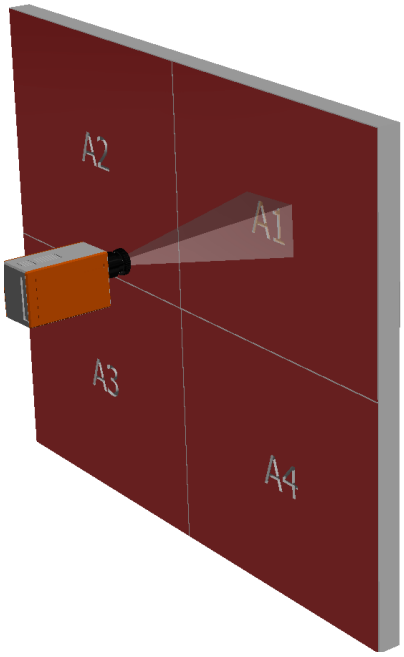

Figure 5.12: Defined inspection areas of reference specimen A2, respectively coded with A1 to A4

A DFT is performed at the frequencies of 0.7 Hz, 0.5 Hz, 0.3 Hz, 0.1 Hz, 0.05 Hz and 0.03Hz. As a result, the DFT provides for every pixel the amplitude and phase information at different frequencies. Figure 5.13 presents phase information, showing the influence of the DFT at the different frequencies on the test results for inspection area A2 in more in detail. Inspection area A2 includes the impacts x1.20, +3.20 and +5.40, and the foil locations T1,1,c , T2,1,c and T3,1,c.

- At the DFT of 0.7 Hz, the foil locations could be detected from the phase image, although the indication at the 0.25 inch foil diameter is doubtful. The impact locations could be detected clearly in a cloverleaf shape.
- At the DFT of 0.5 Hz, the foil locations cannot be classified as detectable anymore. The appearance of the impact locations are quite similar compared to 0.7 Hz test result.
- At the DFT of 0.3Hz, the foil locations showed comparable detectability w.r.t. the DFT of 0.7 Hz. At the DFT of 0.7 Hz, the foil area was presented in lighter grey color compared to the sound material. At the DFT of 0.3 Hz, this is reversed (phase transition frequency). At the DFT of 0.3 Hz, the impact locations starts to take shape of a more uniform and round defect area.
- At the DFT of 0.1 Hz, the foil locations show the most contrast compared to sound material. The impact locations are presented in a more circle pattern, yet the contrast for the impact locations $x^{1.20}$ and $+^{3.20}$ has become lower.

- For the DFT frequencies of 0.05 Hz and 0.03 Hz, a reduction of contrast can be observed for both the foil and impact locations.

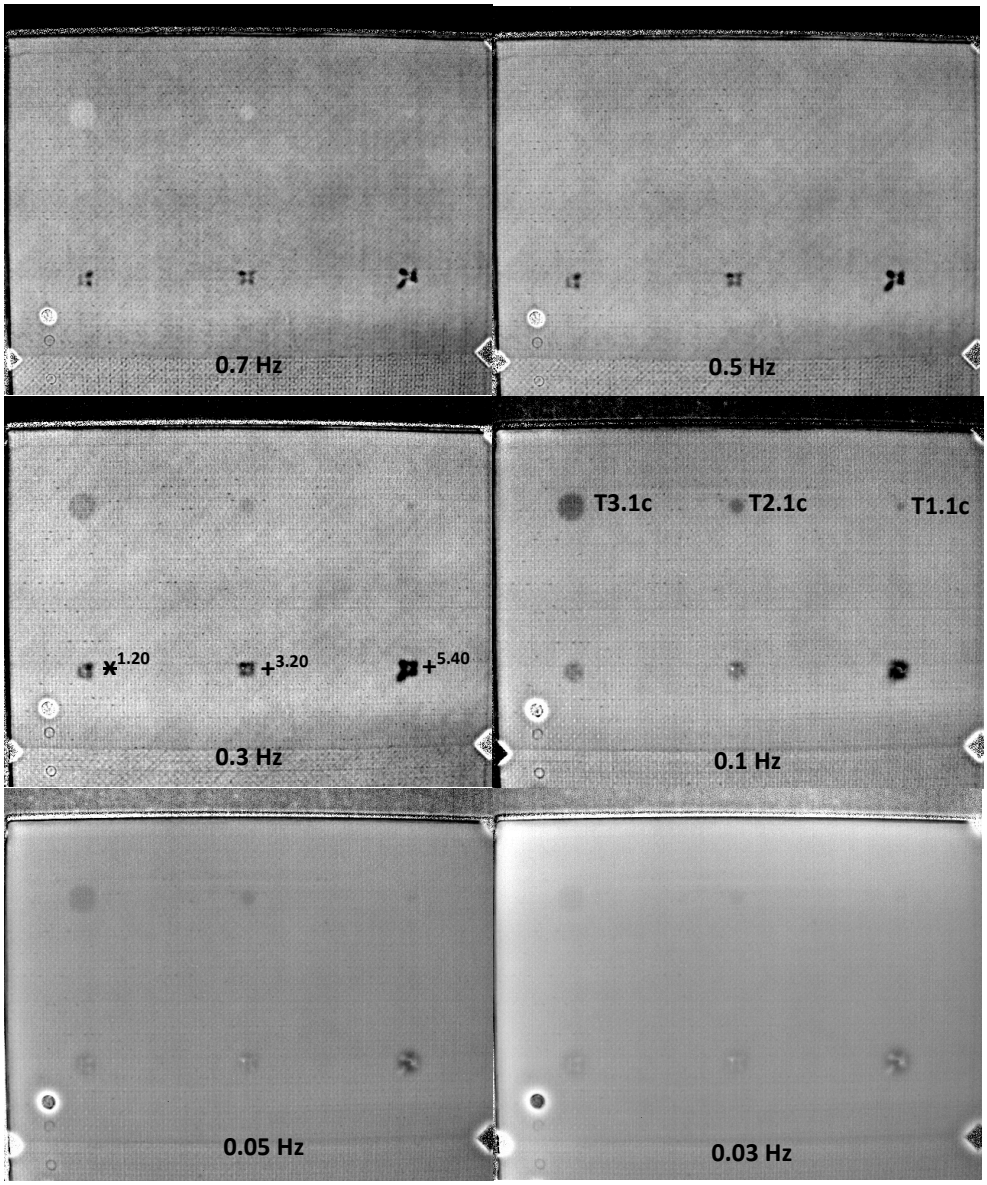

Figure 5.13: Phased images after DFT at the different frequencies, inspection area A-A2

Figure 5.14 shows the influence of the selected DFT frequencies on the test results for the complete specimen. The following general observations of reference specimen A2 can be made:

- All impact locations could be detected successfully. No significant influence can be observed w.r.t. detectability between the different frequencies. The delaminations, caused by impact, have somewhat cloverleaf shape at the frequencies 0.7, 0.5 and 0.3 Hz. At the lower frequencies of 0.05 and 0.03 Hz, a more circle pattern can be observed but with a lower contrast.
- Foil locations with diameters of ¼, ½ and 1 inch diameter at a depth of 0.7 mm could be detected successfully. Optimum frequency is found to be at 0.1 Hz.
- Foil locations at depths of 2.0, 3.4 and 4.7 mm could not be detected.
- No significant differences could be found between the test results with and without copper mesh.

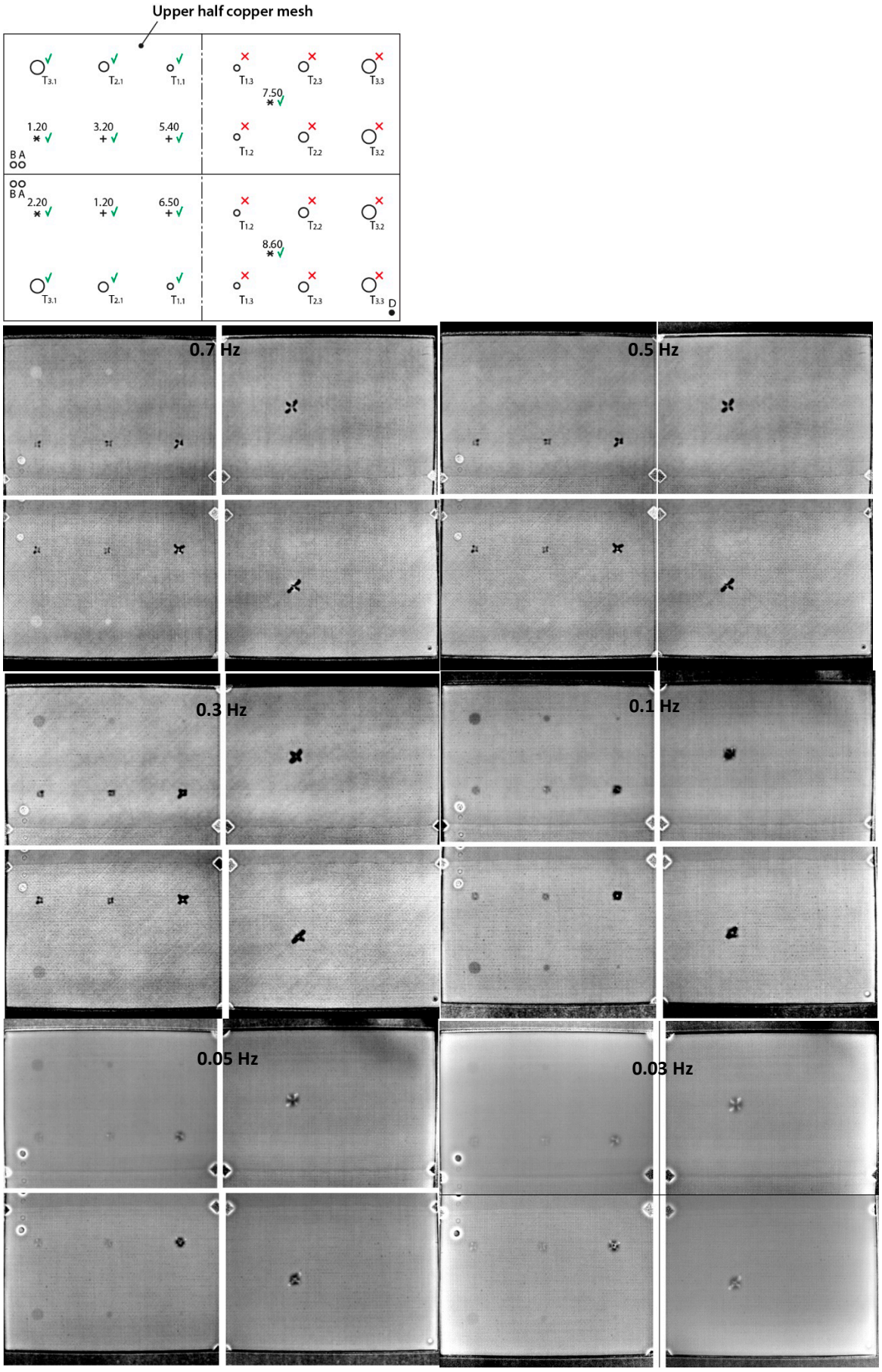

Figure 5.14: Phase images after applying DFT for the different frequencies for specimen A2

Table 5-5 shows a summary of the test results on the test specimen A2. When a defect is detected, a SNR value is determined. Furthermore, the actual sizes of the artificial defects are provided, which can be compared to the measured sizes of the detected defects acquired by thermography. To determine the detectability and sizing capability of the thermography method w.r.t. real impact delamination, ultrasonic data is used as a reference

Table 5-5: Measured SNR of the defect of reference specimen A2, using PT

Reference specimen A2			Pulse Thermography (PT)											
	Defect type	Actual size	SNR [Hz]						Measured size w/h [mm] @ corresponding frequency [Hz]					
		Dia./ depth [mm]	0.7	0.5	0.3	0.1	0.05	0.03	0.7	0.5	0.3	0.1	0.05	0.03
With copper mesh	T1,1,c	6.35/0.7			1.7	3.6	1.5		5x5		5x5	6x6	6x6	
	T2,1,c	12.7/0.7	1.3		1.3	4.2	1.8		12x12		12x12	12x12	12x12	
	T3,1,c	25.4/0.7	2.6		1.4	5.7	1.5		25x25		25x25	25x25	25x25	
	T1,2,c	6.35/3.4												
	T2,2,c	12.7/3.4												
	T3,2,c	25.4/3.4												
	T1,3,c	6.35/4.7												
	T2,3,c	12.7/4.7												
	T3,3,c	25.4/4.7												
	✱[1.20]	31x30	1.6	2.5	3.2	2.3	0.7	0.0	16x17	16x17	16x17	20x18	20x18	25x25
	+[3.20]	18x23	2.9	3.9	4.4	2.6	1.3	1.3	19x15	19x15	19x16	21x17	22x22	23x23
	+[5.40]	32x31	5.3	8.1	10.6	9.3	7.2	6.5	23x23	23x23	23x24	25x26	26x29	33x36
	✱[7.50]	42x38	5.5	8.1	10.2	8.8	4.8	4.0	28x30	28x30	28x30	28x30	28x30	28x30
Without copper mesh	T1,1	6.35/0.7	0.4			2.0	1.9		7x7			7x7	7x7	
	T2,1	12.7/0.7	1.4			3.2	2.5	0.7	12x12			12x12	12x12	12x12
	T3,1	25.4/0.7	1.6		1.5	3.4	1.3	2.3	28x28		28x28	28x28	28x28	28x28
	T1,2	6.35/3.4												
	T2,2	12.7/3.4												
	T3,2	25.4/3.4												
	T1.3	6.35/4.7												
	T2.3	12.7/4.7												
	T3.3	25.4/4.7												
	✱[2.20]	31x29	2.2	3.7	4.8	2.5	0.3	1.3	16x17	16x19	17x20	16x18	16x18	20x23
	+[4,20]	21x27	1.6	2.9	4.1	3.1	1.5	1.5	16x16	15x16	15x16	17x17	19x20	22x25
	+[6.50]	37x29	7.0	13.2	22.1	18.6	9.6	4.9	25x23	27x25	27x25	23x23	27x25	29x28
	✱[8.60]	42x40	3.0	5.6	9.2	7.7	5.0	3.6	30x31	32x31	35x32	31x30	33x32	36x35

- **Sizing ability foils:**
  The foils (at 0.7 depth) could be sized quite well compared to the nominal size. Only T3.1, a foil with a nominal diameter of 25.4 mm, was estimated approximately 3 mm oversized. Considering that this estimation is based on the calibrated results, the defect sizing seems to be reasonably good.
- **Sizing ability impacts:**
  A general statement w.r.t. the sizing ability of the impacts is hard to make. The phase images from the DFT for the higher frequencies (0.7, 0.5, 0.3 Hz) showed in general significantly under sizing of the impact damage compared to the ultrasonic pulse-echo data. Because of the multilayer delamination appearance through the thickness, it is most likely that only the upper part of the delamination could be detected by the PT at higher frequencies. The phase images from the DFT of the lower frequencies (0.1, 0.05 and 0.03Hz) showed in general a larger indication of the impacts closer to the nominal size of the ultrasonic pulse-echo data, see Figure 5.15

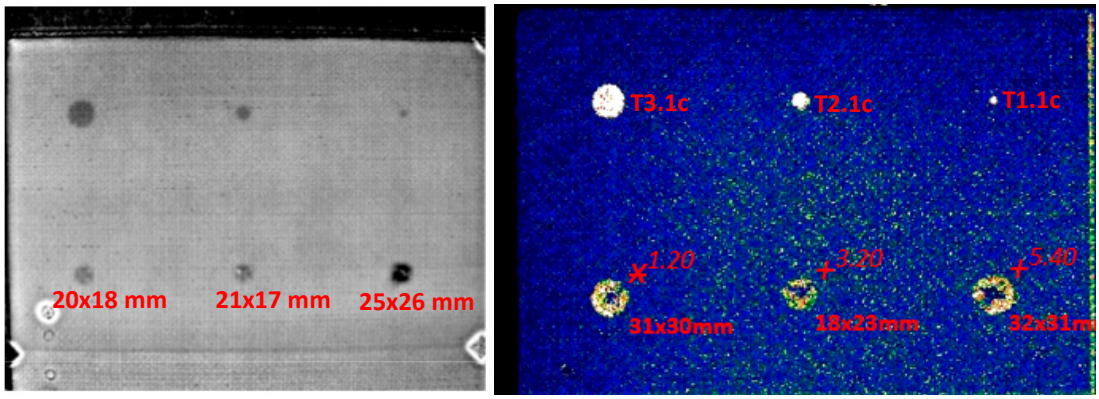

Figure 5.15: DFT at 0.1 Hz and ultrasonic pulse-echo reflection C-scan test results of area A2

5.2.2 Reference specimen C

A PT inspection was performed on the complete reference specimen C. For the complete measurement report, the reader is referred to [11]. In this study, the ROI was ¼ of the surface area respectively coded with C-A1 to C-A4, see Figure 5.16 In this case, a flash excitation was performed, a heating pulse of relatively short duration (<< 1 sec) to create a disrupted thermal balance.

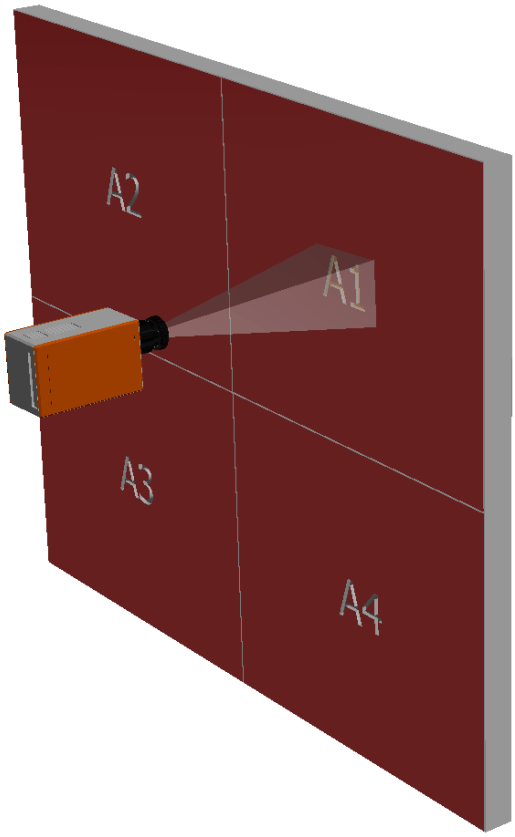

Figure 5.16: Defined inspection areas of reference specimen C, respectively coded with C-A1 to C-A4

A DFT is performed at the frequencies of 0.7 Hz, 0.5 Hz, 0.3 Hz, 0.1 Hz, 0.05 Hz and 0.03Hz. As a result, the DFT provides for every pixel the amplitude and phase information at different frequencies.

Figure 5.17 presents phase information, showing the influence of the DFT at the different frequencies on the test results for inspection area C-A2 in more detail. Inspection area C-A2 includes the impact $+^{1.20}$, foil locations T1,1,c, T2,1,c and T3,1,c, skin-to-honeycomb core disbonds HD2, HD3 and HD4, water ingress in the Nomex honeycomb cells W1, W4 and W5.

- At the DFT of 0.7 Hz, the foil locations and the skin-to-honeycomb core disbonds could not be detected from the phase image. On the other hand, the impact location $+^{1.20}$ was clearly detectable.
- At the DFT of 0.5 Hz, more or less the same test result as for the DFT of 0.7 Hz.
- At the DFT of 0.3 Hz, the foil location T3,1,c could be detected but with a low contrast. Furthermore, clear indication of the impact was observed and a doubtfull indications of the water ingress W4 and W5 were visible.
- At the DFT of 0.1 Hz, more or less the same test result were achieved as for the DFT of 0.3 Hz.
- At the DFT of 0.05 Hz, foil location T3,1,c could not be detected anymore. On the other hand, optimum detectability of the water ingress W4 and W5 and skin-to-honeycomb core disbonds HD3 and HD4 were achieved with this frequency.
- It is noted that skin-to-honeycomb core disbonds HD2 could not be detected in any of the applied DFT frequencies.
- Between the DFT of 0.05 Hz and 0.03 Hz, the grey color of the defects were reversed (phase transition frequency).

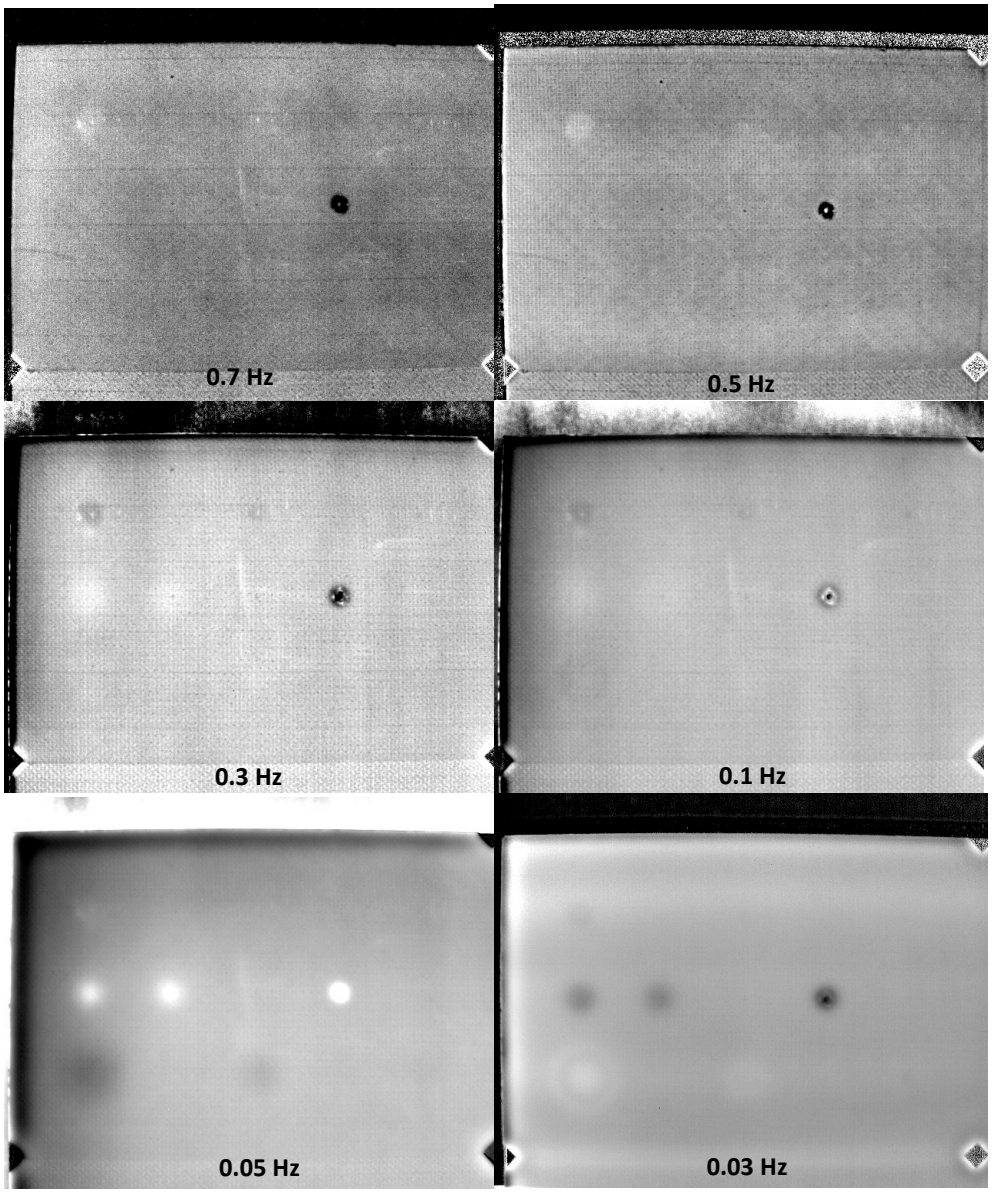

Figure 5.17: Phased images after DFT at the different frequencies, inspection area C-A2

Figure 5.18 shows the influence of the selected DFT frequencies on the test results for the complete specimen. The following general observations of reference specimen C can be made:

- All impact locations could be detected successfully. No significant influence can be observed w.r.t. detectability between the different frequencies applied to. The delaminations have somewhat cloverleaf shape at the frequencies 0.7, 0.5 and 0.3 Hz. At the lower frequencies 0.05 and 0.03 Hz, a more circle pattern could be observed.
- Only the foil locations with a diameter of 1 inch at a depth of 1.5 mm could be detected with limited contrast (with and without copper mesh). Optimum frequencies to detect the foils were found to be in the range of 0.3 and 0.1 Hz.
- The foil diameters 0.25 and 0.5 inch at the depth of 1.5 mm could not be detected.
- All diameter foils (0.25, 0.5 and 1 inch) at a depth of 2.25 mm could not be detected.
- The 1 and 2 inch diameter skin-to-honeycomb core disbonds (HD3 and HD4) at the depth of 3 mm could be detected at the DFT frequencies 0.1, 0.05 and 0.03Hz. However, skin-to-honeycomb core disbonds of a ¼ and ½ inch (HD1 and HD2) could not be detected at a depth of 3 mm. At the DFT at the frequency 0.03Hz, the indication of the disbond appeared as multiple circles.
- The water ingress in the Nomex honeycomb cells W4 and W5 could be detected.
    - Remark: The filling of the cells with water was performed in 2015 [10]. Due to possible diffusion of the water through the Nomex cells, the artificial water ingress defects should be treated as unreliable. Even though W4 and W5 could be detected successfully, no further analysis was performed.
- No significant differences could be observed between the test results with and without copper mesh.

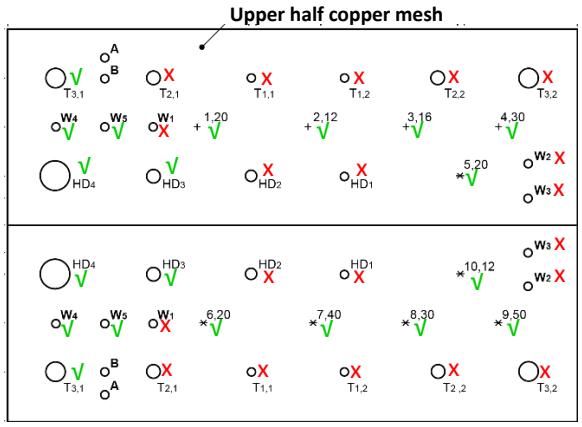

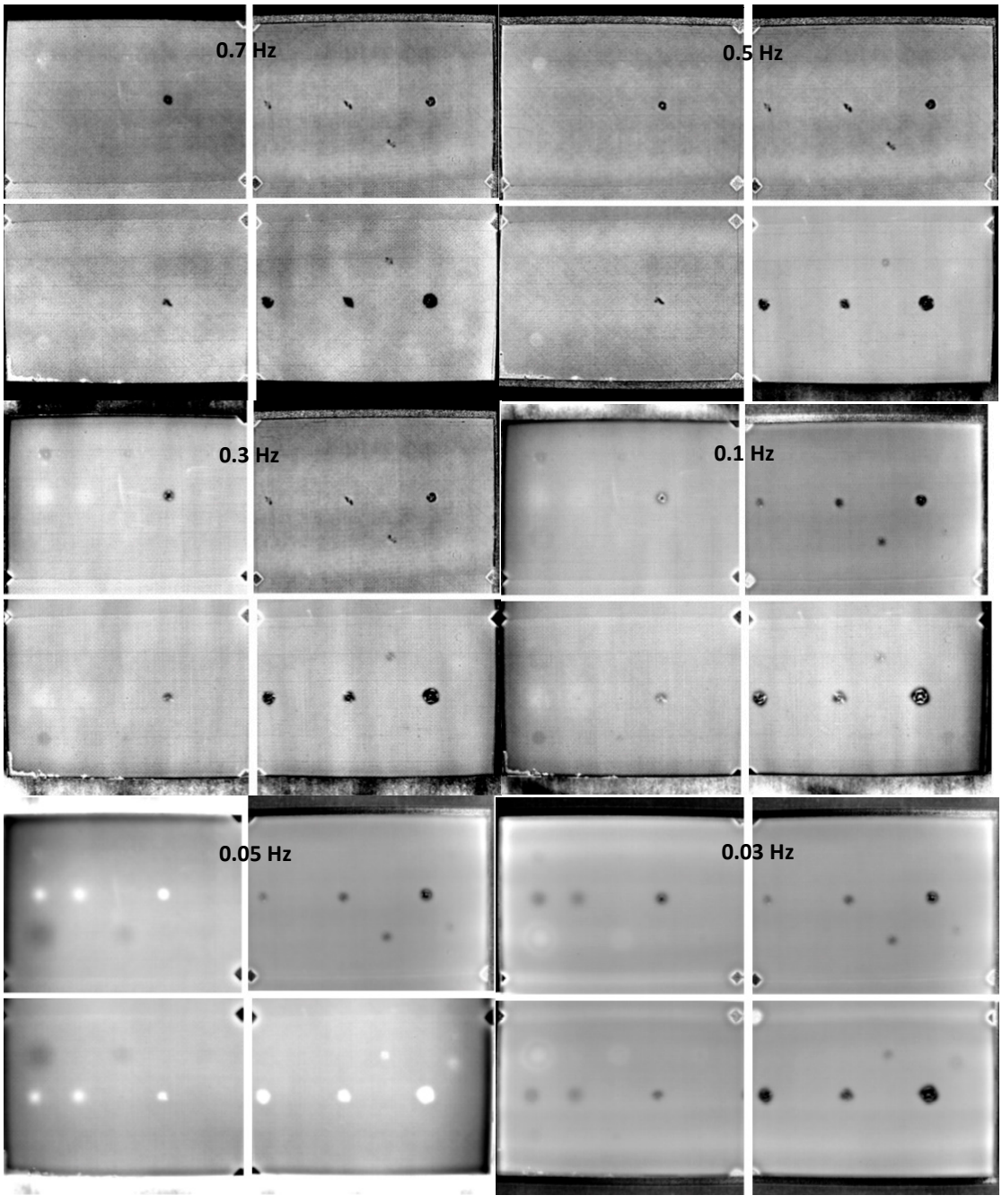

Figure 5.18: Phased images after applying DFT for the different frequencies for specimen C

Table 5-6 shows a summary of the test results. When a defect is detected, a SNR value is determined. Furthermore, the actual sizes of the artificial defects are provided, which can be compared to the measured sizes of the detected defects acquired by thermography. To determine the detectability and sizing capability of the thermography method w.r.t. real impact delamination, ultrasonic data is used as a reference.

Table 5-6: Measured SNR of the defect of reference specimen C using PT

Reference specimen C			Pulse Thermography (PT)											
	Defect type	Actual size	SNR [Hz]						Measured size w/h [mm] @ corresponding frequency [Hz]					
		Dia./ depth [mm]	0.7	0.5	0.3	0.1	0.05	0.03	0.7	0.5	0.3	0.1	0.05	0.03
With copper mesh	T1,1,c	6.35/1.5												
	T2,1,c	12.7/1.5												
	T3,1,c	25.4/1.5			2.5	3.6	5.1				27x31	23x26	22x24	
	T1,2,c	6.35/2.25												
	T2,2,c	12.7/2.25												
	T3,2,c	25.4/2.25												
	HD1	6.35/3.0												
	HD2	12.7/3.0												
	HD3	25.4/3.0				1.9	3.5	1.4				25x27	30x30	35x35
	HD4	50.8/3.0				8.0	12.9	13.3				45x48	50x50	50x50
	+[1,20]	PE 20x19 TT 54x60	9.9	12.1	14.4	20.5	23.9	29.5	18x20	18x19	19x20	23x23	30x30	34x34
	+[2,12]	PE 17x18 TT 54x57	2.6	3.3	3.7	4.5	8.4	7.3	15x18	15x18	16x19	19x21	22x24	22x23
	+[3,16]	PE 23x20 TT 60x62	2.9	5.2	8.4	11.0	16.2	15.6	17x19	17x19	17x21	21x22	27x26	30x29
	+[4,30]	PE 25x23 TT 64x66	16.1	21.7	28.2	28.7	31.0	31.4	18x18	20x18	20x18	25x25	32x32	34x38
	⁎[5,20]	PE 23x21 TT 77x77	2.3	3.5	5.5	8.5	13.6	13.5	20x18	20x18	20x18	24x23	32x28	32x28
Without copper mesh	T1,1	6.35/1.5												
	T2,1	12.7/1.5												
	T3,1	25.4/1.5			1.7	1.5	0.3				27x29	27x29	27x29	
	T1,2	6.35/1.5												
	T2,2	12.7/2.25												
	T3,2	25.4/2.25												
	HD1	6.35/2.25												
	HD2	12.7/3.0												
	HD3	25.4/3.0				1.4	3.5	0.1				25x25	25x25	35x35
	HD4	50.8/3.0				7.5	12.7	8.2				45x45	45x45	60x60
	⁎[6,20]	PE 26x23 TT 74x72	2.8	4.5	6.8	9.5	14.5	12.9	20x18	21x18	21x18	21x19	28x25	29x26
	⁎[7,40]	PE 35x36 TT 85x87	4.9	9.6	16.6	27.2	38.7	45.8	25x22	24x27	22x22	25x25	22x25	32x33
	⁎[8,30]	PE 33x26 TT 83x77	3.7	8.0	13.7	20.8	27.9	30.4	23x22	21x22	19x20	23x24	22x24	27x25
	⁎[9,50]	PE 45x41 TT 81x81	6.9	13.8	24.6	37.2	43.7	49.3	27x28	27x27	28x29	32x32	30x30	42x40
	⁎[10,12]	PE 20x20 TT 57x55	1.2	2.4	3.2	5.0	8.7	8.8	15x13	15x12	15x15	16x18	16x17	19x19

- **Sizing ability foils:**
  The foils could be sized quite well compared to the nominal size. Foil T3.1 (at 1.5 mm depth) with a nominal diameter of 25.4 mm was sized in the range from 22 to 29 mm. Considering that this estimation is based on the calibrated results, the defect sizing seems to be reasonably good.

- **Sizing ability impacts:**
  A general statement w.r.t. to the sizing ability of the impacts is hard to make. The phase images from DFT for the higher frequencies (0.7, 0.5, 0.3 and 0.1 Hz) provide in general significantly undersized damage estimation compared the ultrasonic pulse-echo data. Because of the multilayer delamination appearance through the thickness, it is most likely that only the upper part of the delamination could be detected by the PT at higher frequencies. The phase images from the DFT of the lower frequencies (0.05 and 0.03 Hz) showed in general a larger determination of the impacts closer to the nominal size of the ultrasonic pulse-echo data. When the sizing of the thermography data is compared to the through-transmission C-scan, the impact damages are significantly undersized by the PT. Possible cause could be that skin-to-core disbonds around the impact locations are not detected by the PT. It is noted that the artificial skin to honeycomb disbonds were detectable with OLT (see the next bullet point). On the other hand, the through-transmission C-scan data shows not a complete attenuation of the sound beam at the impact location which is an indication that the core is not completely separated from the skin.
- **Sizing ability Skin-to-honeycomb core disbonds:**
  The Skin-to-honeycomb core disbond HD03 with a nominal size of 1 inch was measured ranging from 25 to 35 mm depending on the used DFT frequency. The HD04 with a nominal size of 2 inch was measured ranging from 45 to 60 mm depending on the used DFT frequency. For both HD04 locations at the DFT at 0.03Hz frequency, the indication of the disbond has an appearance of multiple circles which makes exact sizing more difficult.

6 Discussion

When comparing the thermography methods (both lock-in and pulse) with the ultrasonic method, it is noted that thermography is fast and non-contact inspection method and needs no complex scanning equipment. On the other hand, the detectability of thermography method is in general lower, especially with increasing defect depth. The panels up to 1 m^2 could be inspected with a single measurement. However, the FOV of 450 x 300 mm is chosen in this study. Chapter 5 of this report describes the test results of the thermography method for both optical lock-in and pulse on the relatively large composite reference specimens. The test results are acquired based on in-service conditions (e.g. one-sided access). The two specimens consist of a solid thermoset laminate and a thermoset sandwich panel with a Nomex core. The test specimen contain the following type of defects; impact damage, inserted single foils, skin-to-honeycomb core disbonds and water ingress at honeycomb core. Figure 6.1 shows an overview of detectability results achieved with both thermography methods on both solid and honeycomb sandwich specimens. When other aspects, such as signal-to-noise ratios and sizing, are not taken into account, the test results of the solid panel A2 are exactly the same for the both methods. For the sandwich specimens, the lock-in method scores better, the blue circles indicates the differences. In general, the lock-in thermography demonstrated a somewhat better performance compared to the pulse method. The lock-in method also shows slightly better signal-to-noise ratios. For both methods applies that the detectable defect size decreases with an increasing defect depth.

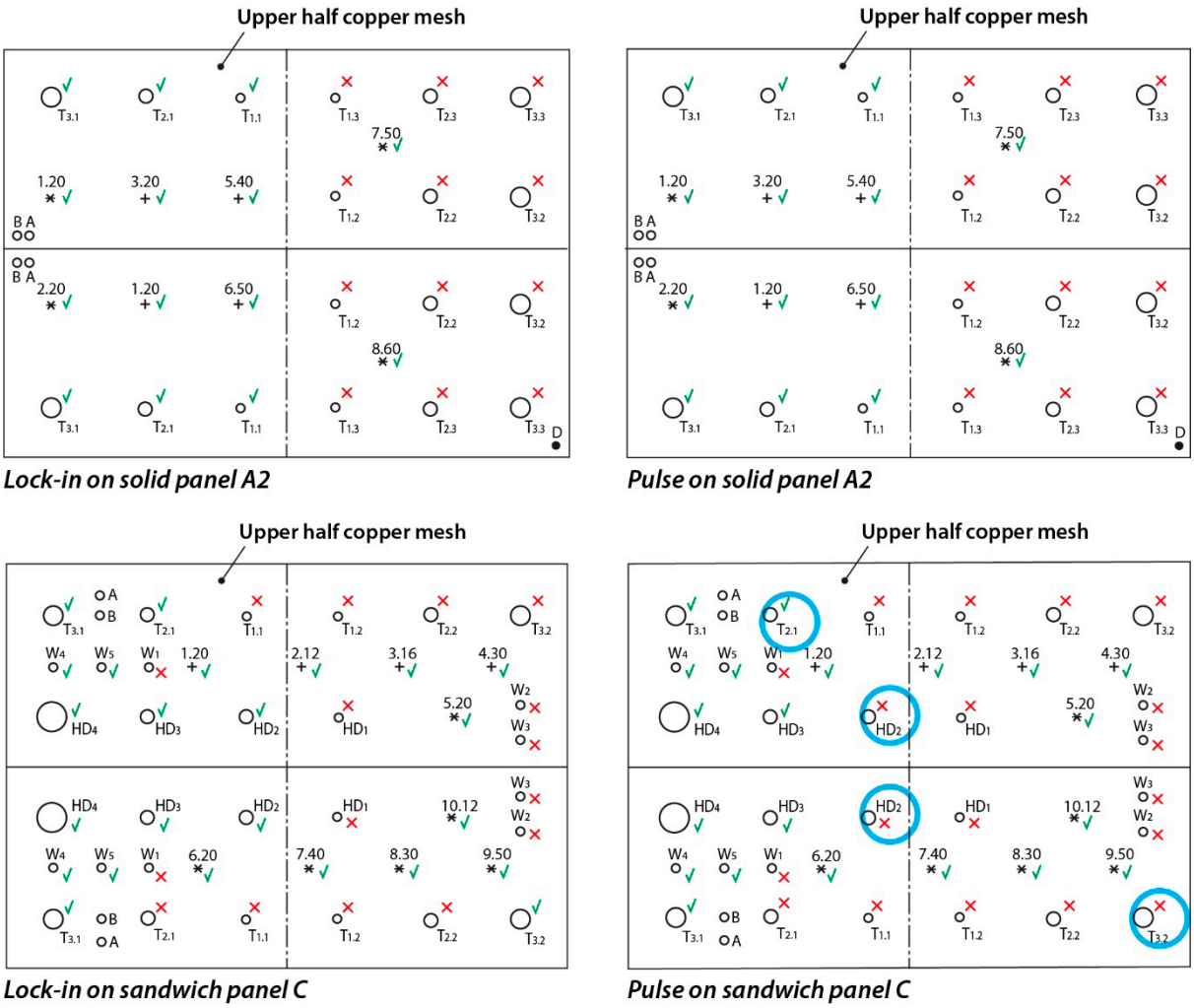

Figure 6.1: Comparison optical lock-in versus pulse thermography on composite reference specimens A2 and C

For both panels and both thermography methods, it is remarkable that only the foil locations close to the surface < 2 mm depth are detectable with exception of foil location T3.2 at specimen C at a depth of 2.25 mm. Foil locations at 3.4 and 4.7 mm depths are not detectable. On the other hand, the skin-to-core disbonds at a depth at 3 mm are detectable. When simulating a delamination made from single layer foil material, it is possible that the defects have not created a full separation of the individual laminate layers during the manufacturing process. This is less relevant for e.g. UT inspection (any interface with different acoustic impedance can be detected) but very relevant for the thermography inspection. When observing the ultrasonic through-transmission data of Figure 6.2, it can be seen that no 100 % attenuation occurs at the foil locations. This is an indication that the foils are adhered to the composite layers.

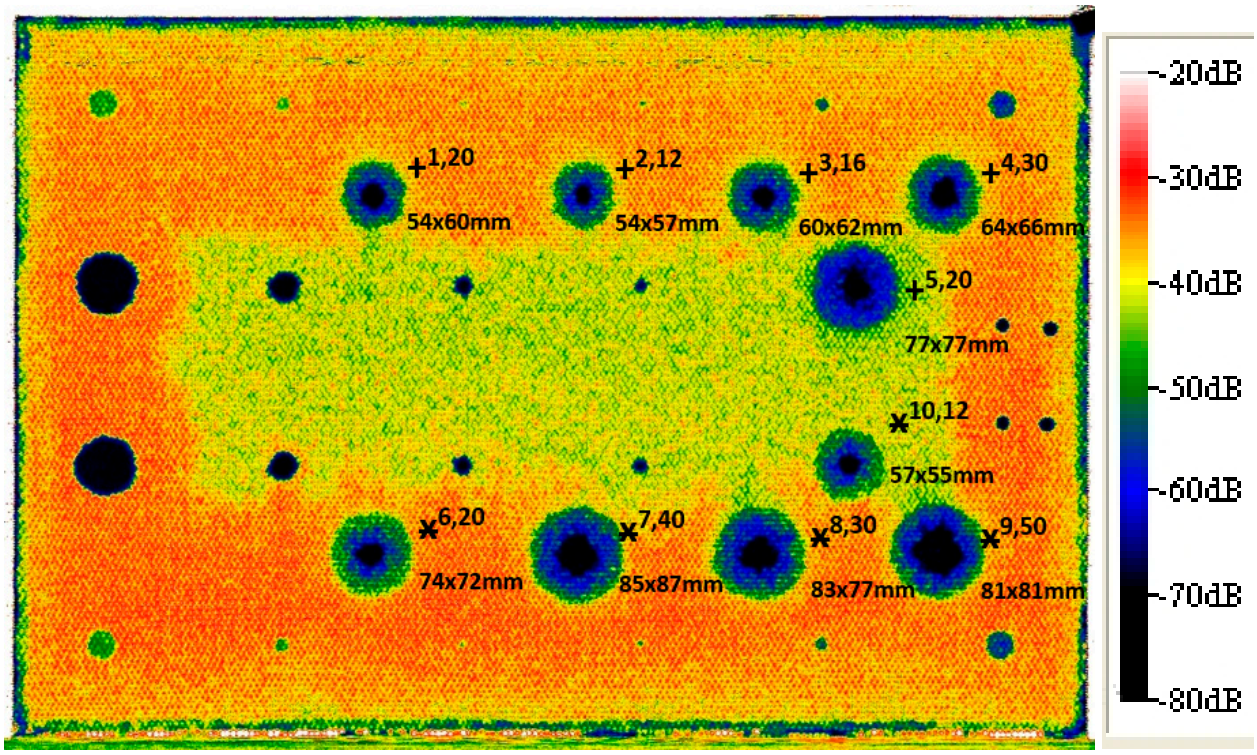

Figure 6.2: Specimen C, ultrasonic through-transmission data of the impact damage locations

There is a significant difference in the percentage heat reflection between composite/Teflon (18.9%) and composite/air (98.4%). These reflection values are valid for the thermography method and calculated using the thermal effusivity of the two materials and air, see Section 4.3 equation (4.7). It is recommended to investigate alternative ways to create artificial defects simulating a representative delamination at a defined depth for the thermography method. Examples of alternative methods could be to use double-sided foils sealed at the edges or pull tabs.

When the sizing of the thermography data is compared to the through-transmission C-scan, the impact damages are significantly undersized. Possible cause could be that skin-to-core disbonds around the impact locations is not detected, this is contrary with the artificial skin to honeycomb disbonds which are detectable with thermography. On the other hand, the through-transmission C-scan data shows not a complete attenuation of the sound beam at the impact location which is an indication that the core is not completely separated from the skin.

7 Conclusions

1. Thermography inspection method is portable, fast-operating and non-contact way of performing NDI. Thermography inspection has a large FOV (~1m^2) and this method is applicable from a single side and is therefore suitable for in-service inspections.
2. The method is only suitable for relative thin composite structures up to about 5-6 mm.
3. The evaluation of thermography showed that the method is well capable of detecting impact damage which is the most severe in-service damage that can occur to a composite structure.
4. Inserted Teflon foils could be detect to a maximal depth of approximately 2 mm. Possible reason that deeper positioned foils are not detected is that the foils are adhered to the adjacent composite layers instead of a full separation of the individual laminate layers.
5. Larger artificial skin-to-core disbonds (> 1inch) could be detected reliably by the thermography method.
6. The detectable defect size decreases with increasing defect depth (defect diameter must exceed its depth).
7. Estimation of the defect size is accurate enough.
8. In general, the lock-in thermography demonstrated a somewhat better performance compared to the pulse method. The lock-in method also shows slightly better signal-to-noise ratios.
9. Evaluation in the frequency domain (Fast Fourier Transformation (FFT) or a Discrete Fourier Transform (DFT)) eliminates for a great part disturbances, such as reflections from the surface and thermal imbalance from the inspection room. Therefore, the thermography method is well suited for inspections under hangar conditions when the data is analysed in frequency domain.
10. Thermography is possibly a cost-effective inspection method for first screening of large composite areas for both solid and sandwich structures. When more detailed information is needed, the ultrasonic method can be used at deviant areas appointed by the thermography inspection.
11. The high end xenon flash lamps and the special generator to generate a short burst signal make the pulse thermography equipment more expensive in comparison to lock-in thermography. Furthermore, safety precautions must be taken to prevent serious eye injuries caused by xenon flash lamps.
12. The thermography method is an ideal partner in a multi-domain approach, e.g. in combination with shearography and 3D structural light scanning (not considered in this evaluation).

8 References

1. Heida, J.H.; "*DCMC WP2 NDO methoden*", NLR memorandum AVGS-2018-004, February 2018;
2. Rademakers, E.R.; Platenkamp, D.J.; *"Round Robin NDT results with laser ultrasonic equipment of various providers in the DCMC project"*, NLR-CR-2019-100;
3. Jansen, H.P.; "Introducing shearography as a complementary NDT-technique at NLR", A NLR deliverable of the DCMC-project, NLR-CR-2019-513;
4. Hyll, K.; "*Image-Based Quantitative Infrared Analysis and Microparticle Characterisation for Pulp and Paper Applications*", PhD Thesis, KTH Royal Institute of Technology, Stockholm, Sweden, 2016, DOI: 10.13140/RG.2.1.2595.6884;
5. Heida, J.H.; Platenkamp, D.J.; "*Evaluation of non-destructive inspection methods"*, NLR-CR-2010-076, 2010;
6. Norman Walker, J.; "*BINDT CM series Infrared Thermography Principles and Practice"*, volume 1, 2004;
7. Meola, C. ; Boccardi , S.; Carlomagno, GM.; "*Infrared thermography in the evaluation of aerospace composite materials"*, Woodhead Publishing, ISBN 978-1-78242-171-9, 2015;
8. Kalter, L.R.; "*Characterisation of damage in composite materials using infrared thermography*", MSc Thesis, University of Twente, Enschede, the Netherlands, 2018;
9. Zweschper, Th; Koch, J.; "*Non-destructive inspection of CFRP components by means of optically excited lock-in thermography (OTvis)"*, Stuttgart, 23.10.2018, Report # 19124921.001;
10. Heida, J.H.; Platenkamp, D.J.; Bosch, A.F., D.J.; "*In-service inspection of water ingress in composite honeycomb structures"*, NLR-CR-2015-278, 2010;
11. Zweschper, Th ; Koch, J.; "*Non-destructive inspection of CFRP components by means of pulse thermography (flash excitation) (PTvis)"*, Stuttgart, 23.10.2018, Report # 19124921.002.

Appendix A **Composite specimens**

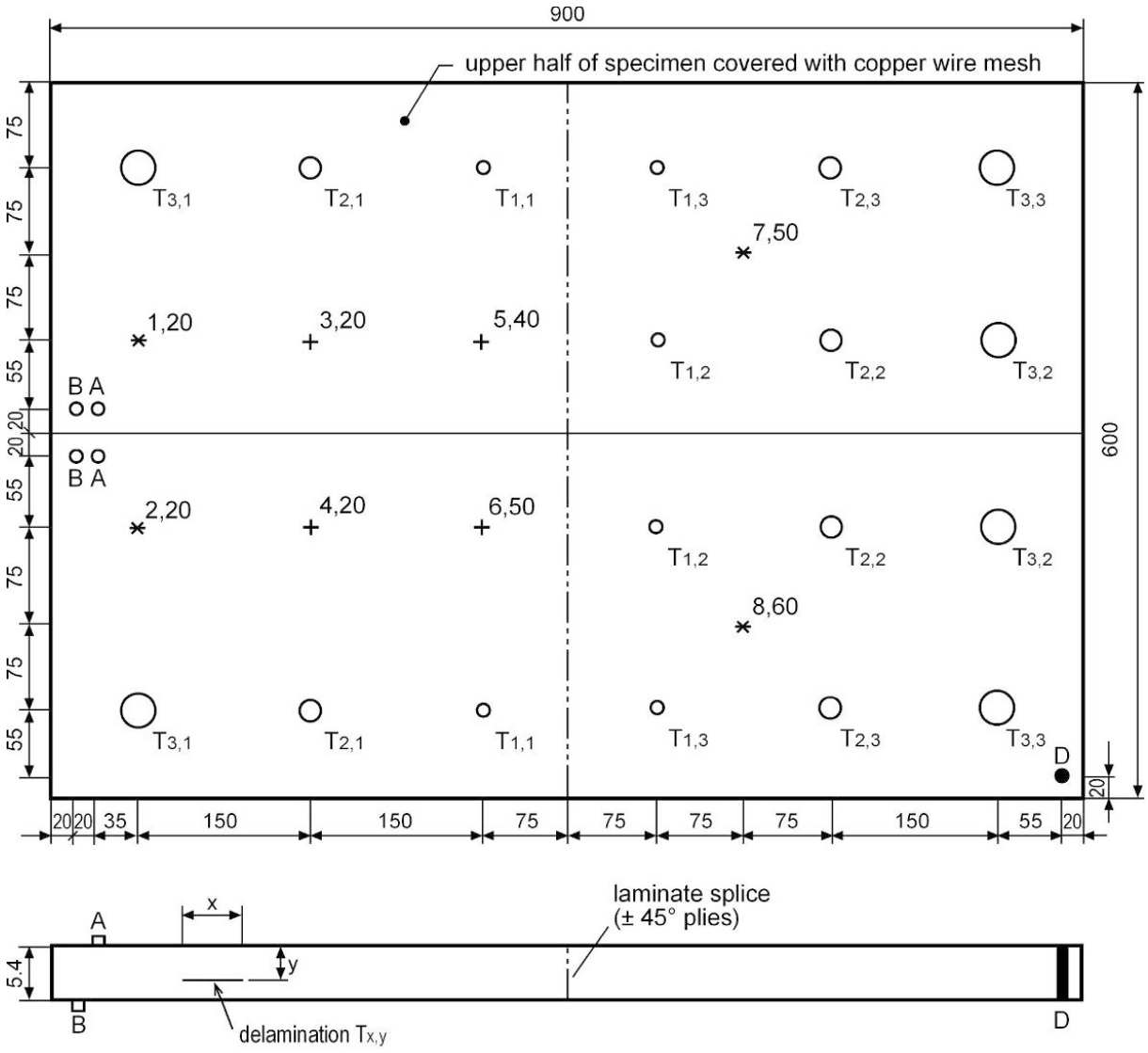

Defect type	
Delamination $T_{x,y}$	x = 1, 2 or 3 Diameter 0.25; 0.5 or 1.0 inch y = 1, 2 or 3 Depth 0.7; 3.4 or 4.7 mm
Impact $+^{x,y}$ $*^{x,y}$	+ / * Impactor tup diameter 0.5/1.0 inch x = Impact number; y = Impact energy [J]
Adhesive sticker	A ∅ 8 mm on top side of laminate B ∅ 8 mm on bottom side of laminate
Hole D	∅ 8 mm

*Figure A.1: Specimen **A2**, solid laminate with artificial delaminations and low-velocity impact damages*

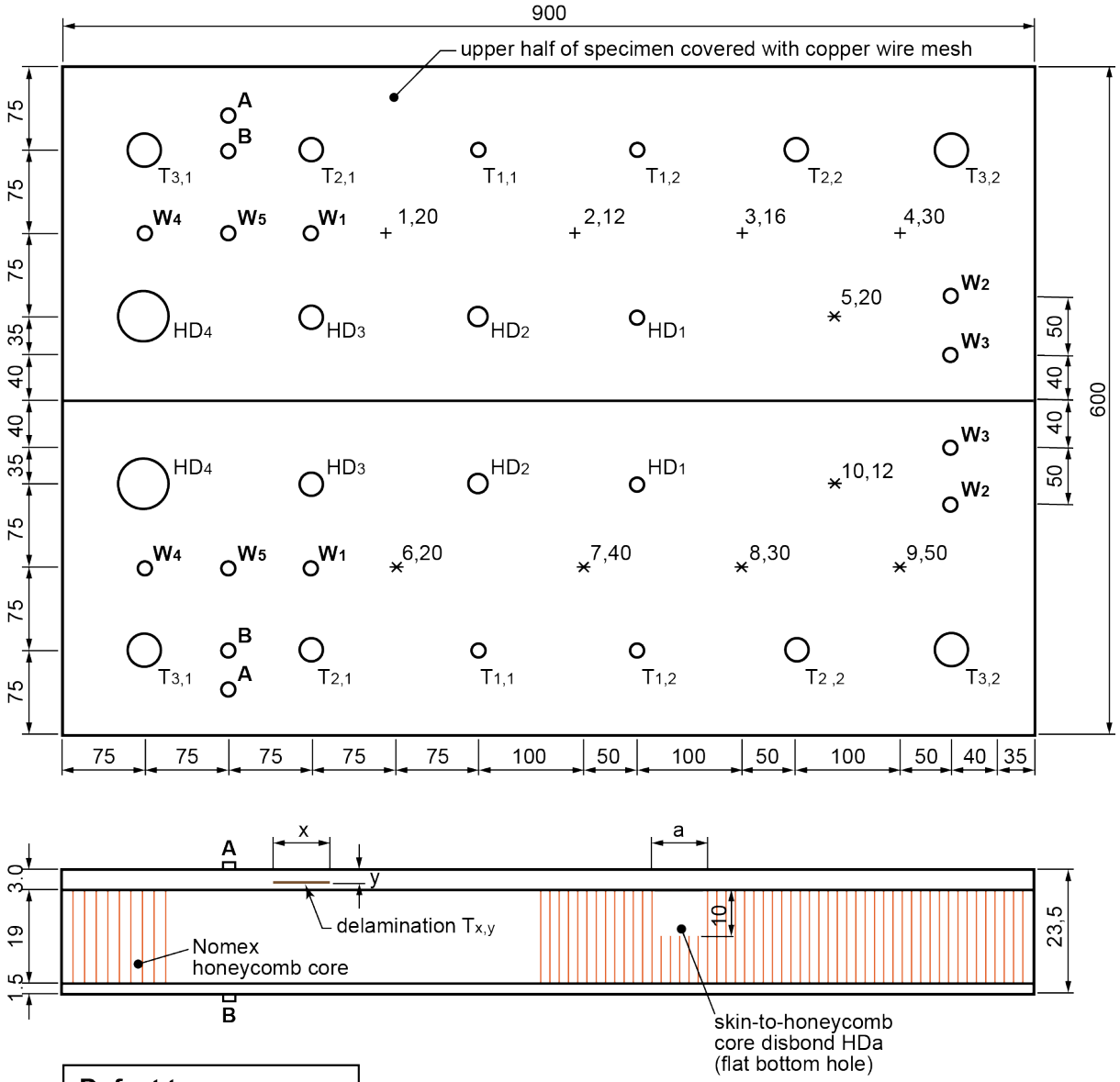

Defect type		
Delamination $T_{x,y}$	x = 1, 2 or 3 y = 1 or 2	Diameter 0.25; 0.5 or 1.0 inch Depth 1.5 or 2.25 mm
Skin-to-honeycomb core disbond HDa	a = 1, 2, 3 or 4	Diameter 0.25; 0.5; 1.0 or 2.0 inch
Impact $+^{x,y}$ $*^{x,y}$	+ /* Impactor tup diameter 0.5/1.0 inch x = Impact number; y = Impact energy [J]	
Adhesive sticker	A ∅12 mm on outer skin B ∅12 mm on inner skin	
Water ingress Wx in honeycomb cells (HC)	x = 1 1 HC full x = 2 3 HC full x = 3 3 HC half-full x = 4 7 HC full x = 5 7 HC half-full	

Figure A.2: Specimen C, sandwich structure with artificial delaminations in the outer skin, outer skin-to-honeycomb core disbonds, low-velocity impact damages and water ingress in the Nomex honeycomb cells

Dedicated to innovation in aerospace

Royal NLR - Netherlands Aerospace Centre

NLR operates as an objective and independent research centre, working with its partners towards a better world tomorrow. As part of that, NLR offers innovative solutions and technical expertise, creating a strong competitive position for the commercial sector.

NLR has been a centre of expertise for over a century now, with a deep-seated desire to keep innovating. It is an organisation that works to achieve sustainable, safe, efficient and effective aerospace operations.
The combination of in-depth insights into customers' needs, multidisciplinary expertise and state-of-the-art research facilities makes rapid innovation possible. Both domestically and abroad, NLR plays a pivotal role between science, the commercial sector and governmental authorities, bridging the gap between fundamental research and practical applications. Additionally, NLR is one of the large technological institutes (GTIs) that have been collaborating over a decade in the Netherlands on applied research united in the TO2 federation.

From its main offices in Amsterdam and Marknesse plus two satellite offices, NLR helps to create a safe and sustainable society. It works with partners on numerous programmes in both civil aviation and defence, including work on complex composite structures for commercial aircraft and on goal-oriented use of the F-35 fighter. Additionally, NLR helps to achieve both Dutch and European goals and climate objectives in line with the Luchtvaartnota (Aviation Policy Document), the European Green Deal and Flightpath 2050, and by participating in programs such as Clean Sky and SESAR.

For more information visit: **www.nlr.org**

Postal address
PO Box 90502
1006 BM Amsterdam, The Netherlands
e) info@nlr.nl **i)** www.nlr.org

Royal NLR
Anthony Fokkerweg 2
1059 CM Amsterdam, The Netherlands
p) +31 88 511 3113

Voorsterweg 31
8316 PR Marknesse, The Netherlands
p) +31 88 511 4444